PROCEEDINGS A

royalsocietypublishing.org/journal/rspa

Research

Cite this article: Hu Y, Schaeffer D.G, Barker T. 2024 Onsager-symmetric constitutive laws for three-dimensional granular flow in the inertial regime. *Proc. R. Soc. A* **480**: 20230955.
https://doi.org/10.1098/rspa.2023.0955

Received: 23 December 2023
Accepted: 2 October 2024

Subject Category:
Mathematics

Subject Areas:
fluid mechanics, applied mathematics, geophysics

Keywords:
granular flow, continuum modelling, rheology

Author for correspondence:
T. Barker
e-mail: BarkerT1@cardiff.ac.uk

Electronic supplementary material is available online at https://doi.org/10.6084/m9.figshare.c.7577968.

Onsager-symmetric constitutive laws for three-dimensional granular flow in the inertial regime

Y. Hu[1], D.G. Schaeffer[2] and T. Barker[3]

[1]School of Mathematical Sciences, Shanghai JiaoTong University, Shanghai 200240, People's Republic of China
[2]Mathematics Department, Duke University, Box90320, Durham, NC 27708-0320, USA
[3]School of Mathematics, Cardiff University,Senghennydd Road, Cardiff, CF24 4AG, UK

TB, 0000-0001-9403-0435

This paper introduces a new mathematical technique for deriving continuum rheological models of granular matter. Specifically, it is shown that, under the hypothesis of Onsager symmetry, three-dimensional dynamic constitutive laws for general strain rates can be derived from a three-dimensional yield condition plus steady-state empirical data of quasi-two-dimensional flow. To illustrate the technique, a new rate-dependent three-dimensional yield condition, suitable for dry granular materials in the inertial regime, is proposed and combined with discrete-element method (DEM) particle simulation data of simple shear flow. In combination with Onsager symmetry, this generates a complete three-dimensional viscoplastic model for such materials. Despite the simplicity of the inputs, the resulting constitutive laws agree very well with the pioneering non-planar DEM simulations of Clemmer *et al*. *Phys. Rev. Lett*. **127** (2021). Unlike several previous theories, the novel Onsager-symmetric constitutive relations incorporate a non-zero second normal stress difference in simple shear and are able to distinguish between general triaxial deformations via dependence on the Lode angle.

THE ROYAL SOCIETY PUBLISHING

royalsocietypublishing.org/journal/rspa Proc. R. Soc. A 480: 20230955

1. Introduction

The main purpose of this paper is to demonstrate a surprising consequence of Onsager symmetry: in the context of viscoplastic modelling of particulate flows, partial three-dimensional constitutive information—specifically, a yield condition—can be extended to complete three-dimensional constitutive relations using only certain empirical two-dimensional rheological data. Here this technique is illustrated via one specific choice of three-dimensional yield condition appropriate for granular flow in the inertial regime.

Onsager's theory of the thermodynamics of irreversible processes [1] prescribes a precise balance of variations between conjugate pairs of micro-state 'forces' and 'fluxes' in order that dissipation is minimized. These reciprocal relations therefore represent a unique and powerful ingredient both for deriving and for closing governing equations. Indeed, many theories across soft matter physics [2], continuum mechanics [3] and in the thermodynamic description of granular materials [4] already utilize Onsager symmetry in various ways. Here the nonlinear Onsager symmetry of Edelen [5], which, as processed by Goddard & Lee [6], corresponds to partial differential equations linking principal stresses to their dependence on the principal strain rates, will be employed. While it remains unclear whether real granular materials actually possess Onsager symmetry, information about the consequences of Onsager symmetry, such as the present paper, may help resolve this issue.

Attention here will be limited to granular materials composed of monodispersed hard spheres of diameter d and density ρ_*. Only liquid-like inertial flow, in which the solid volume fraction ϕ lies in an intermediate range $0.4 \lesssim \phi \lesssim 0.6$ between the gaseous and quasi-static solid-like regimes [7], will be considered. Two features of inertial flow—Bagnold scaling [8], in which stresses scale with the square of strain rates, and $\Phi(I)$-rheology [9,10], whereby the solid volume fraction and inertial number I are functions of one another in steady planar flow—will form key ingredients of the theory.

To illustrate the application of Onsager symmetry and to go beyond the previous two-dimensional theories, such as $\mu(I)$, $\Phi(I)$-rheology [9,11] and compressible I-dependent rheology (CIDR) [12], a new three-dimensional yield function is proposed. Like the Lade–Duncan and the Matsuoka–Nakai criteria [13], this includes dependence on the stress Lode angle [14], describing non-planar triaxial aspects of the flow. However, unlike in incompressible rate-independent models [15], the new yield condition also includes dependence on ϕ and I as in the two-dimensional inertial compressible I-dependent rheology (iCIDR) [16].

Given that the yield condition depends on the stress Lode angle, it follows that the stress and strain-rate Lode angles are independent variables. In particular, the constitutive laws predict that the second normal stress difference *in planar simple shear* is non-zero. Further implications of the new theory are illustrated for a range of non-planar flows, matching those detailed in the discrete-element method (DEM) particle simulations of Clemmer *et al*. [17]. By first fitting their data for simple shear flow, the new theory is able to make close predictions of non-planar constant-volume flow data which were not used in the fitting. This suggests that many assumptions used in the construction of the model, including Onsager symmetry, are realistic. In fact, the new theory makes predictions for arbitrary three-dimensional deformation rates, including for unsteady flows with non-zero compression/dilation rate. Testing these predictions poses a future challenge for experiments and/or simulations.

The derivation of the constitutive laws relies on interesting, unfamiliar, mathematics. Specifically, we shall see that the combination of a yield condition with Onsager symmetry leads to an over-determined system of algebro-differential equations. The occurrence of an over-determined system may help motivate one surprising aspect of this paper—that complete three-dimensional constitutive information can be deduced from partial three-dimensional information plus certain two-dimensional results.

The paper is organized as follows. Section 2 describes in detail the necessary definitions for working with three-dimensional flows and defines precisely the constitutive assumptions

from which the equations are derived. Section 3 reports the final constitutive relations and demonstrates their usage, implications for a range of typical flows and provides comparison with the DEM data of Clemmer *et al*. [17]. Section 4 details the full derivation of the constitutive relations, working from what are known as the characteristic ODEs. Section 5 summarizes the conclusions and discusses some related issues. Four appendices are included which cover the following: appendix A, in which the characteristic equations are derived using differential geometry; appendix B, which analyses the three-dimensional yield condition; appendix C, in which the method of fitting DEM data is detailed; appendix D, which contains certain technical proofs that would be distracting in the main body of the paper. Proofs of convexity of the dissipation potential are included in electronic supplementary material I and extensions of the theory to include suspensions and generalized yield surfaces are detailed in electronic supplementary material II.

2. Modelling inputs and definitions

In this section, the four main inputs of our model: material isotropy with an ordering principle, Onsager symmetry, $\Phi(I)$-rheology for steady simple shear and a yield condition, are introduced along with a review of cylindrical coordinates for the stress and strain-rate eigenvalues.

(a) Isotropic constitutive laws with an ordering principle

We consider granular flow in three spatial dimensions. To fix notation, let $\boldsymbol{\sigma}$ denote the stress tensor, $\boldsymbol{u}$ the velocity field, $\boldsymbol{D} = (\nabla \boldsymbol{u} + \nabla \boldsymbol{u}^T)/2$ the strain-rate tensor and ϕ the volume fraction. The pressure is defined by $p = -\mathrm{tr}\,\boldsymbol{\sigma}/3$ and $\boldsymbol{\tau} = \boldsymbol{\sigma} + p\boldsymbol{1}$ is the shear stress tensor. Volumetric changes are described by the rate of dilation $q = \mathrm{tr}\,\boldsymbol{D} = \mathrm{div}\,\boldsymbol{u}$, and the remaining aspects of the deformation rate by the deviatoric strain-rate tensor $\boldsymbol{S} = \boldsymbol{D} - (q/3)\boldsymbol{1}$. Tensor norms are defined by $\|\boldsymbol{T}\| = \sqrt{T_{ij}T_{ij}/2}$, for any tensor $\boldsymbol{T}$, such that $\tau = ||\boldsymbol{\tau}||$ is the shear stress and $s = ||\boldsymbol{S}||$ is the shear rate.

By *constitutive law* we mean here a continuous function

$$\boldsymbol{\sigma} = \boldsymbol{\Sigma}(\boldsymbol{D}, \phi) \tag{2.1}$$

that relates the stress tensor with the strain-rate tensor and volume fraction. This rules out, for example, dependence on spin [18], fabric [19], non-locality [20], fluctuations [21,22] and history [23]. Once specified, equation (2.1) may be paired with mass and momentum conservation to generate closed-form equations of motion; however in this work, we do not explore this, instead focussing on the rheological behaviour in isolation.

In the following, several hypotheses will be made for such a constitutive law. To begin with, we assume that the tensor function $\boldsymbol{\Sigma}(\boldsymbol{D}, \phi)$ is *isotropic* in $\boldsymbol{D}$; that is,

$$\boldsymbol{\Sigma}(\boldsymbol{R}\boldsymbol{D}\boldsymbol{R}^T, \phi) = \boldsymbol{R}\boldsymbol{\Sigma}(\boldsymbol{D}, \phi)\boldsymbol{R}^T, \tag{2.2}$$

for any orthogonal matrix $\boldsymbol{R}$. According to [24, pp. 32–33], such a $\boldsymbol{\Sigma}(\boldsymbol{D}, \phi)$ admits a representation formula[1]

$$\boldsymbol{\Sigma}(\boldsymbol{D}, \phi) = a\boldsymbol{1} + b\boldsymbol{D} + c\boldsymbol{D}^2, \tag{2.3}$$

where a, b and c are functions of the invariants of $\boldsymbol{D}$ and ϕ. Thus, the stress and strain-rate tensors are simultaneously diagonalizable and equation (2.1) is completely determined by the inter-relations between the three eigenvalues of stress σ_i and the three eigenvalues of strain rate D_i such that

$$\sigma_i = \Sigma_i(D, \phi), \qquad \text{for} \qquad i = 1,2,3, \tag{2.4}$$

where D is a vector shorthand for (D_1, D_2, D_3). Moreover, we assume that[2]

$$\sigma_i < \sigma_j < \sigma_k \quad \text{whenever} \quad D_i < D_j < D_k. \tag{2.5}$$

Constitutive laws that satisfy both equations (2.2) and (2.5) will be referred to as *isotropic with an ordering principle*.

(b) Onsager symmetry

As detailed in Goddard & Lee [6], based on the work of Edelen [5], isotropic constitutive laws specified by equation (2.4) are said to be *Onsager symmetric* if

$$\frac{\partial \Sigma_i}{\partial D_j} = \frac{\partial \Sigma_j}{\partial D_i}, \qquad (i, j = 1, 2, 3) \quad \text{for } \boldsymbol{D} \notin \mathbb{R}\mathbf{1}. \tag{2.6}$$

The condition '$\boldsymbol{D} \notin \mathbb{R}\boldsymbol{1}$' specifies all strain-rate tensors that are not a multiple of the identity; our reason for including this restriction is to allow $\boldsymbol{\Sigma}$ to be non-smooth near $\mathbb{R}\boldsymbol{1}$.

We remark that, although Onsager symmetry arises in Edelen's nonlinear theory of irreversibility [3,5] and is related to the existence of a dissipation potential, its definition does not rely on the existence of such a potential.

(c) Review of cylindrical coordinates for stress and strain rate

We follow several authors [14,17,25] in using cylindrical coordinates (p, τ, θ) and (q, s, φ) for the stress and strain-rate eigenvalues, respectively, wherein the angular components, θ and φ are the Lode angles. These coordinates are related to the rectangular coordinates by the formulae

$$\begin{aligned}
\sigma_1 &= -p + \tau\left(\cos\theta + \frac{\sin\theta}{\sqrt{3}}\right), & D_1 &= q/3 + s\left(\cos\varphi + \frac{\sin\varphi}{\sqrt{3}}\right),\\
\sigma_2 &= -p + \tau\left(-\cos\theta + \frac{\sin\theta}{\sqrt{3}}\right), & D_2 &= q/3 + s\left(-\cos\varphi + \frac{\sin\varphi}{\sqrt{3}}\right),\\
\sigma_3 &= -p + \tau\left(-\frac{2\sin\theta}{\sqrt{3}}\right), & D_3 &= q/3 + s\left(-\frac{2\sin\varphi}{\sqrt{3}}\right).
\end{aligned} \tag{2.7}$$

Regarding stresses, the pressure measures distance along the line $\{\sigma_1 = \sigma_2 = \sigma_3\}$, which is the '$z$'-axis of cylindrical coordinates; τ, θ represent polar coordinates in a plane $\{p = \text{const}\}$. Simple shear is characterized by $q = 0$ and $\varphi = 0$. In the constitutive laws developed below, θ is non-zero in simple shear even though $\varphi = 0$.

Note that the quantities

$$\sin 3\theta = \frac{\sqrt{27}\,\det \boldsymbol{\tau}}{2\tau^3} \quad \text{and} \quad \sin 3\varphi = \frac{\sqrt{27}\,\det \boldsymbol{S}}{2s^3} \tag{2.8}$$

are invariants of $\boldsymbol{\sigma}$ and $\boldsymbol{D}$, respectively, but θ and φ are not—which value is appropriate depends on the ordering of the relative eigenvalues. For instance, $\sigma_2 < \sigma_3 < \sigma_1$ corresponds to the principal range[3] $\theta \in [-\pi/6, \pi/6]$, similarly $D_2 < D_3 < D_1$ to $\varphi \in [-\pi/6, \pi/6]$, where the minimum and maximum values correspond to triaxial compression and triaxial expansion, respectively.

Another key result for cylindrical coordinates comes from following the appendix of [26] and writing the representation formula (equation (2.3)) as a linear system

$$\boldsymbol{M}\begin{bmatrix} a \\ b \\ c \end{bmatrix} = \begin{bmatrix} \sigma_1 \\ \sigma_2 \\ \sigma_3 \end{bmatrix}, \qquad \text{where} \qquad \boldsymbol{M} = \begin{bmatrix} 1 & D_1 & D_1^2 \\ 1 & D_2 & D_2^2 \\ 1 & D_3 & D_3^2 \end{bmatrix}, \tag{2.9}$$

which, by inverting $\boldsymbol{M}$ and substituting equation (2.7), allows us to derive general formulae for the coefficients

royalsocietypublishing.org/journal/rspa Proc. R. Soc. A 480: 20230955

$$a = -\frac{9ps^2\cos(3\varphi) - \sqrt{3}q^2\tau\sin(\theta-\varphi) + 6\sqrt{3}s^2\tau\sin(\theta-\varphi) + 3qs\tau\cos(\theta+2\varphi)}{9s^2\cos(3\varphi)}, \tag{2.10a}$$

$$b = \frac{3s\tau\cos(\theta+2\varphi) - 2\sqrt{3}q\tau\sin(\theta-\varphi)}{3s^2\cos(3\varphi)}, \tag{2.10b}$$

$$c = \frac{\sqrt{3}\tau\sin(\theta-\varphi)}{s^2\cos(3\varphi)}. \tag{2.10c}$$

As will be demonstrated in §3, these formulae allow for convenient use of the representation formula to construct the stress tensor for general three-dimensional flow.

(d) $\Phi(I)$-rheology for steady simple shear

For steady simple shear, the $\mu(I)$,$\Phi(I)$-rheology [10,11] establishes that the volume fraction ϕ is a function of the inertial number

$$I = \frac{2ds}{\sqrt{p/\rho_*}}, \tag{2.11}$$

such that

$$\phi = \Phi(I). \tag{2.12}$$

The simple linear function

$$\Phi(I) = \phi_c - \frac{I}{I_*}, \tag{2.13}$$

where ϕ_c (the critical density) and I_* are constants, is sufficiently accurate for most purposes. Let $\Psi(\phi)$ be the inverse relation, for equation (2.13),

$$I = \Psi(\phi) = I_*(\phi_c - \phi). \tag{2.14}$$

Substituting the definition (2.11) into this equation and solving for p yields an expression for the pressure in steady simple shear

$$p_{SS} = 4\rho_* d^2\left[\frac{\|\boldsymbol{S}\|}{\Psi(\phi)}\right]^2. \tag{2.15}$$

Thus, any constitutive law that is compatible with $\Phi(I)$-rheology must satisfy: whenever $q = \varphi = 0$, the pressure is given by equation (2.15).

(e) Yield conditions in three dimensions

(i) The Lade–Duncan and Matsuoka–Nakai yield conditions

In three dimensions, the popular Lade–Duncan and Matsuoka–Nakai conditions [13] may both be written in terms of the solution of a cubic equation

$$\beta(\phi)\hat{r}^3\sin(3\theta) + \hat{r}^2 = Y(\phi), \tag{2.16}$$

where

$$\beta(\phi) = \begin{cases} 2/\sqrt{27}, & \text{Lade–Duncan,} \\ (3 - Y(\phi))/\sqrt{27}, & \text{Matsuoka–Nakai,} \end{cases} \tag{2.17}$$

and $Y(\phi)$ reflect the internal friction of the flow.

If material is flowing, these yield conditions require that

$$\frac{\tau}{p} = \hat{r}(\theta, \phi), \tag{2.18}$$

where $\hat{r}(\theta, \phi)$ is the only positive root of equation (2.16) if $\sin(3\theta) > 0$, and the smaller positive root if $\sin(3\theta) < 0$. In appendix B, we show that provided

$$0 < \beta < \beta_0(Y) := \frac{2}{\sqrt{27Y}}, \tag{2.19}$$

which we assume throughout, the solution set of equation (2.16) in the r, θ-plane has a unique bounded component.

(ii) A rate-dependent yield condition

For isotropic constitutive laws, a direct consequence of equation (2.3) is that $\boldsymbol{\Sigma}(\boldsymbol{D}, \phi)$ is a multiple of the identity whenever $\boldsymbol{D}$ is; in other words, if there is no distinguished direction in strain-rate space, there should be no distinguished direction in stress space either. This property cannot be achieved with the rate-independent yield conditions (equation (2.16)); thus, we seek a rate-dependent modification of equation (2.16).

Inspired by the two-dimensional iCIDR theory [16], we assume a three-dimensional yield condition defined in terms of the appropriate solution $r(\theta, I, \phi)$ of

$$\beta(\phi)\left(\frac{\Psi(\phi)}{I}\right) r^3 \sin(3\theta) + r^2 = Y(\phi)\left(\frac{I}{\Psi(\phi)}\right)^2. \tag{2.20}$$

If material is flowing, the yield condition requires that

$$\frac{\tau}{p} = r(\theta, I, \phi). \tag{2.21}$$

Here, $r(\theta, I, \phi)$ relates to the solution $\hat{r}(\theta, \phi)$ of equation (2.16) via

$$r(\theta, I, \phi) = \hat{r}(\theta, \phi)\frac{I}{\Psi(\phi)}. \tag{2.22}$$

Clearly, $\|\boldsymbol{S}\| = 0$ implies $I = 0$ and $\tau = 0$. Also note that, in steady simple shear, $I/\Psi(\phi) = 1$, and equation (2.20) reduces to equation (2.16). Furthermore, taking $\beta = 0$ corresponds to the ϕ-dependent form of the $\mu(I)$,$\Phi(I)$-rheology [16,27] with $\sqrt{Y(\phi)}$ acting as the $\mu(\Psi(\phi))$ relation.

Without appealing to any particular physical insights, beyond curve fitting (as detailed in appendix C), here the functions

$$\Psi(\phi) = I_*(\phi_c - \phi), \tag{2.23}$$

$$Y(\phi) = Y_0 + (Y_\infty - Y_0)\tanh(\Gamma_Y \Psi(\phi)), \tag{2.24}$$

$$\beta(\phi) = \beta_0 + (\beta_\infty - \beta_0)\tanh(\Gamma_\beta \Psi(\phi)), \tag{2.25}$$

are chosen for the free ϕ-dependent steady constitutive relations. Incidentally, forms for Y and β inspired by the $\mu(I)$ function of Jop *et al*. [28] were also tried, but found to give worse fits to the data, especially for low values of ϕ, than the tanh forms (equations (2.24) and (2.25)) chosen here. Plots of the functions so obtained for one set of DEM parameters are shown in figure 1.

3. A summary of the main results

Before detailing the full technical analysis, it is illuminating to outline the structure and implications of the new equations which result from a combination of the ingredients in §2. Here these results will be presented alongside DEM simulation data available in the literature. In particular, the work of Clemmer *et al*. [17] provides key data for homogenous non-planar

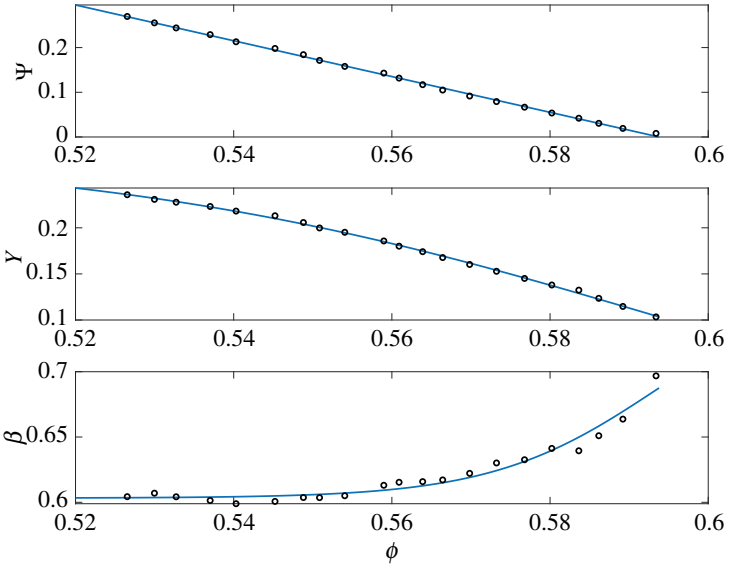

Figure 1. DEM data (open circles) of Srivastava *et al*. [29] compared against the solid line fits of equations (2.23)–(2.25) with parameters listed in table 1.

Table 1. Best fit parameters for the three-dimensional constitutive functions (2.14), (2.24) and (2.25) using the DEM data of Srivastava *et al*. [29]. See figure 1.

$\phi_c = 0.594$	$Y_0 = 0.103$	$Y_\infty = 0.284$	$\Gamma_Y = 3.50$
$I_* = 4.00$	$\beta_0 = 0.688$	$\beta_\infty = 0.603$	$\Gamma_\beta = 11.8$

Table 2. Best fit parameters for the ϕ-dependent constitutive functions (2.14), (2.24) and (2.25) using the DEM data of Clemmer *et al*. [17].

$\phi_c = 0.589$	$Y_0 = 0.112$	$Y_\infty = 0.360$	$\Gamma_Y = 2.93$
$I_* = 3.88$	$\beta_0 = 0.640$	$\beta_\infty = 0.639$	$\Gamma_\beta = 7.54$

($\varphi \neq 0$) flows, albeit only for isochoric cases with $q = 0$. Following the method detailed in appendix C, the coefficients in $\Psi(\phi)$, $\beta(\phi)$ and $Y(\phi)$ are first derived from the simple shear simulations of Clemmer *et al*. [17], leading to the values listed in table 2. While all aspects of the new theory rely on these choices, it is only through synthesis with Onsager symmetry that predictions for non-planar flow can be derived from this simple shear data.

(a) Constitutive relations

We seek constitutive laws that express stress as a function of packing fraction and strain rate as in equation (2.1). Thus, *a priori*, the Lode angle might depend on all three invariants of the full strain-rate tensor, but as we show in §4, it depends only on φ as

$$\theta = \Theta(\varphi, \phi). \tag{3.1}$$

We will also see in §4 that $\Theta(\varphi, \phi)$ is the solution of a system of ODEs and does not have a closed-form expression. Instead, numerical solutions are plotted for some selected packing fractions in figure 2, which match closely with [17].

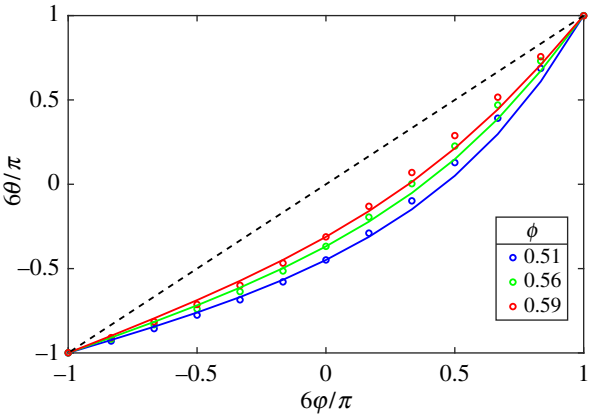

Figure 2. Plots of the stress Lode angle θ as a function of the strain-rate angle φ for a range of packing fractions ϕ. Solid lines are predictions of the new theory, open circles are derived from the DEM data of Clemmer *et al*. [17] (with interparticle friction 0.3) and the black dashed line denotes $\theta = \varphi$. Note that the three simple shear points with $\varphi = 0$ match almost precisely with the theory as they are used in the fitting, whereas all other predictions result consequently owing to the structure of the full theory.

This behaviour differs from constitutive laws [12,28] of the form

$$\tau \propto \frac{\boldsymbol{S}}{||\boldsymbol{S}||}, \tag{3.2}$$

which predict that $\theta = \varphi$. As shown in figure 2, θ and φ are equal only for triaxial expansion $\theta = \varphi = \pi/6$ and triaxial contraction $\theta = \varphi = -\pi/6$, with $\theta < \varphi$ for all intermediate flows in the inertial regime.

The next key outcome of the analysis is the equation of state for the pressure

$$p = P(q, s, \varphi, \phi) = \rho_* d^2 \left[\frac{\sqrt{q^2 + 4Z(0,\phi)Z(\varphi,\phi)s^2} - q}{\Psi(\phi)Z(0,\phi)} \right]^2, \tag{3.3}$$

where

$$Z(\varphi, \phi) = \frac{1}{2}\hat{r}\cos(\Theta - \varphi), \tag{3.4}$$

in which functional dependencies have been hidden from the right-hand side of equation (3.4) for brevity. This new expression equation (3.3) shares many similarities with the equation of state for two-dimensional iCIDR as derived in [16], which, in our present notation, may be written

$$P_{\mathrm{iCIDR}}(s, q, \phi) = \rho_* d^2 \left[\frac{\sqrt{q^2 + \mu(\phi)^2 s^2} - q}{\Psi(\phi)\,\mu(\phi)/2} \right]^2, \tag{3.5}$$

with $\mu(\phi)$ being the steady bulk friction coefficient. Comparison of equation (3.5) with equation (3.3) reveals that the new theory can differentiate between the 'type' of the deformation, as tracked by φ, in addition to the strain-rate magnitude s and compression rate q. Validation of these dependencies via comparison with DEM is reserved for future studies as Clemmer *et al*. [17] fix the pressure and only consider volume-preserving flows with $q = 0$.

Specification of the constitutive relations is completed via an expression for the shear stress

$$\tau = r(\theta, I, \phi)p, \tag{3.6}$$

royalsocietypublishing.org/journal/rspa Proc. R. Soc. A 480: 20230955

which is simply reconstructed from its definition (equation (2.18)), the prediction (equation (2.22)) of the three-dimensional yield condition, and substitution of p and θ from equations (3.1) to (3.3) above.

(b) Consequences for prototypical flows

Consider the steady velocity field in simple shear flow

$$\underline{u} = \dot{\gamma} y \underline{e}_x, \qquad \text{with} \qquad \dot{\gamma} \in \mathbb{R} \setminus \{0\}, \tag{3.7}$$

aligned with the x-axis and varying linearly in the perpendicular coordinate y. This corresponds to a constant solid volume fraction $\phi = \phi_*$, zero compression rate $q = 0$, and a strain-rate tensor

$$\boldsymbol{D} = \begin{bmatrix} 0 & \dot{\gamma}/2 & 0 \\ \dot{\gamma}/2 & 0 & 0 \\ 0 & 0 & 0 \end{bmatrix}, \tag{3.8}$$

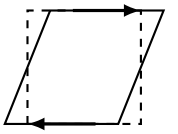

which has constant shear rate $s = |\dot{\gamma}|/2$ and zero polar strain-rate angle $\varphi = 0$. The pressure $p = p_{SS}$ is that given by the $\Phi(I)$-rheology (equation (2.15)), while the new constitutive laws give the stress Lode angle as $\theta_0 = \Theta(0, \phi_*)$ and the magnitude of the shear stress as $\tau = \hat{r}_0 p_{SS}$, where $\hat{r}_0 = \hat{r}(\theta_0, \phi_*)$. Strict two-dimensional alignment (equation (3.2)) would imply that the shear stress tensor $\boldsymbol{\tau}$ is proportional to the strain-rate tensor (equation (3.8)). Instead, three-dimensional alignment, as embodied by the representation formula of equation (2.3), predicts

$$\boldsymbol{\tau} = \begin{bmatrix} \frac{1}{3}cs^2 & bs & 0 \\ bs & \frac{1}{3}cs^2 & 0 \\ 0 & 0 & -\frac{2}{3}cs^2 \end{bmatrix}. \tag{3.9}$$

For the normal stress differences [30–33], which are typically defined as

$$\mathcal{N}_1 = \tau_{11} - \tau_{22}, \qquad \mathcal{N}_2 = \tau_{22} - \tau_{33}, \tag{3.10}$$

the new theory predicts that the first normal stress difference $\mathcal{N}_1 = 0$ vanishes and the second normal stress difference

$$\mathcal{N}_2 = cs^2 = \sqrt{3}\,\hat{r}_0\, p_{SS} \sin(\theta_0), \tag{3.11}$$

using equation (2.10). A normalized second normal stress difference $\mathcal{N}_2/p_{SS}$ is plotted in figure 3, and the other steady stress functions are plotted as black curves in figure 4. These values and trends, which rely on the DEM fitting of the Clemmer *et al*. simple shear flow data [17], are close to those reported elsewhere in the literature [18,29,32,34].

Before considering fully three-dimensional flow, note that the planar bi-axial ('pure shear') deformations

$$\boldsymbol{D} = \begin{bmatrix} \dot{\gamma}/2 & 0 & 0 \\ 0 & -\dot{\gamma}/2 & 0 \\ 0 & 0 & 0 \end{bmatrix}, \tag{3.12}$$

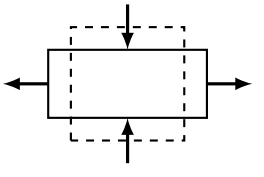

have the same set of strain-rate coordinates as simple shear i.e. $s = |\dot{\gamma}|/2$ and $q = \varphi = 0$. This, therefore, results in the same set of stress coordinates as for simple shear and the two cases are

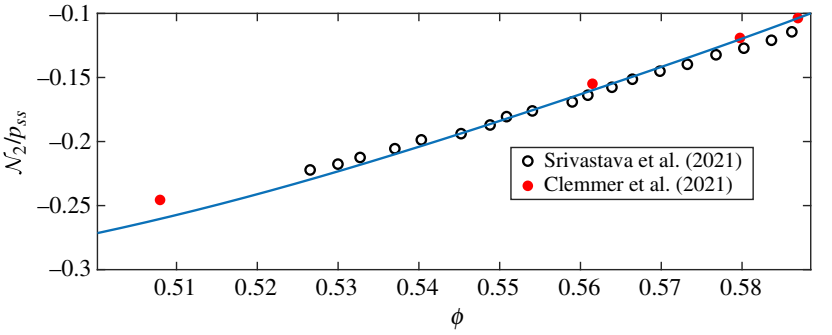

Figure 3. The normalized second normal stress difference $\mathcal{N}_2/p_{ss}$ for simple shear given a range of packing fractions ϕ in the inertial regime. Comparison is made between the new theory (solid line), computed using the right-hand side of equation (3.11), and available data in the literature [17,29] (both with interparticle friction 0.3), computed using equation (3.10), plotted as symbols.

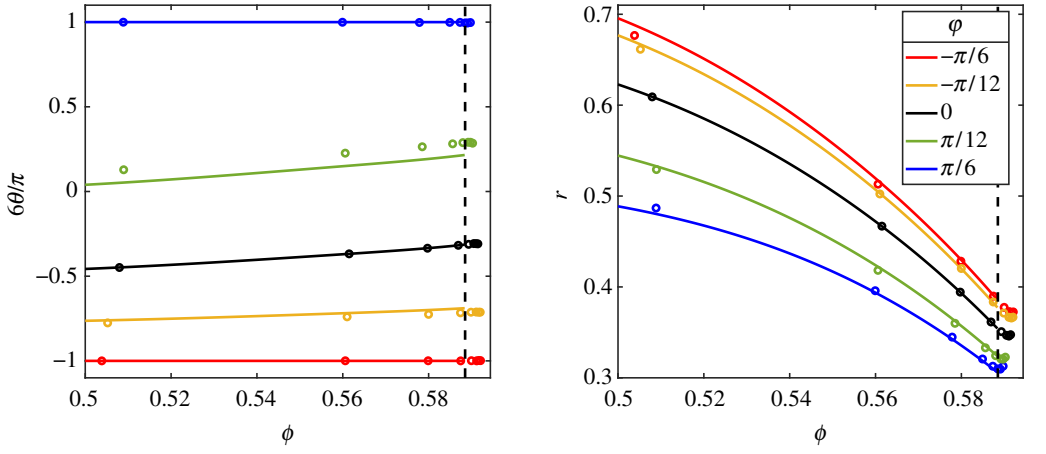

Figure 4. Plots of the stress Lode angle θ and the bulk friction $r = \tau/p$ for a range of triaxial deformations, with different strain-rate Lode angles φ and for a range of packing fractions ϕ. Solid lines are predictions of the new theory and open circles are reproductions of the DEM data of Clemmer *et al.* [17] (with interparticle friction 0.3). Only the black data (simple shear $\varphi = 0$) is used for fitting whereas $\varphi \neq 0$ cases are novel predictions. Vertical dashed lines denote the upper limit of inertial flow $\phi = \phi_c$.

essentially equivalent. This was confirmed by the closely matching DEM simulations of [17] for each type of shear flow and suggests that rotational effects are minimal.

For the fully three-dimensional analogue of equation (3.12) i.e. triaxial deformations described by

$$\boldsymbol{D} = \frac{1}{2\sqrt{3}} \begin{bmatrix} \dot{\gamma} & 0 & 0 \\ 0 & \dot{\gamma} & 0 \\ 0 & 0 & -2\dot{\gamma} \end{bmatrix}, \qquad (3.13)$$

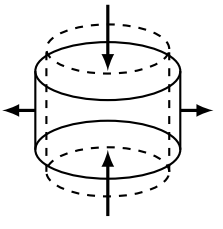

the strain-rate angle $\varphi = \pm\pi/6$ is non-zero, with sign matching the sign of $\dot{\gamma}$, while the other invariants remain the same: $s = |\dot{\gamma}|/2$ and $q = 0$. Figure 4 demonstrates that solutions of our new theory predict significant deviations in the stress fields for these triaxial deformations compared with simple shear, and that these are matched by DEM data.

Finally, it is also interesting to consider the limiting cases of large compression or dilation. The pressure $P(q, s, \varphi, \phi)$, as predicted by the equation of state (equation (3.3)), grows quadratically (as expected from Bagnold scaling) in $|q|$ for compression, i.e. as $q \to -\infty$, and for dilation

$$\lim_{q \to +\infty} P(q, s, \varphi, \phi) = 0.$$

Indeed, for purely volumetric deformations, with $\boldsymbol{D} = (q/3)\boldsymbol{1}$, then

$$p = \begin{cases} C(\phi)q^2, & \text{for} \quad q < 0, \\ 0, & \text{for} \quad q \geq 0, \end{cases} \tag{3.14}$$

where $C(\phi) = \rho_* d^2/(\Psi(\phi)Z(0, \phi))$ comes from evaluating equation (3.3) with $s = 0$.

4. Derivations and proofs

In this section, we derive the constitutive relations given in §3. Because of isotropy (equation (2.2)), it suffices to consider diagonal matrices $\boldsymbol{\sigma}$ and $\boldsymbol{D}$; a constitutive law is then determined by functions $\boldsymbol{\sigma} = \Sigma(\boldsymbol{D}, \phi)$ (equation (2.1)). Thus the objective is to determine three unknown functions Σ_i of the strain rate and ϕ (equation (2.4)), subject to the yield condition (equation (2.20)) and Onsager symmetry (equation (2.6)). The yield condition is a scalar relationship between the three functions; Onsager symmetry is a system of three PDEs. Thus requiring both of these results in a system of four algebro-differential equations for three unknowns—i.e. an over-determined system. A local analysis of such a system can be conveniently handled by Cartan's theory of exterior differential systems [35]. However, since the construction of a constitutive law is global, and in view of the fact that Cartan's theory may not be familiar to most readers, we derive the constitutive relations with ad hoc methods that take advantage of the structure of the system. Even so, our approach is quite geometric, and we put part of the analysis in appendix A, the part that we expect might be an obstacle for readers less acquainted with differential geometry.

In our geometric approach, we view constitutive relations as the following one-parameter family of three-dimensional graphs

$$\mathcal{M}(\phi) = \{(\boldsymbol{\sigma}, \boldsymbol{D}) \in \mathbb{DM}^3 \times \mathbb{DM}^3 : \boldsymbol{\sigma} = \Sigma(\boldsymbol{D}, \phi)\}, \tag{4.1}$$

what we call *constitutive manifolds*. If $\Sigma(\boldsymbol{D}, \phi)$ is Onsager symmetric, then $\mathcal{M}(\phi)$ is also called Onsager symmetric.

(a) Further simplification from isotropy and ordering

The angle θ that is obtained by solving the first of equations (2.8) is sensitive to the ordering of the stress eigenvalues. Assuming no two eigenvalues are equal, there are six such orderings. We divide the space of stress eigenvalues into six wedges $\mathcal{W}_n$ $(n = 1, 2, \ldots, 6)$ corresponding to these orderings. Figure 5 shows the intersection of a plane $\{\sigma_1 + \sigma_2 + \sigma_3 = \text{const}\}$ with the wedges. Each wedge is associated with a range of θ. For example, in

$$\mathcal{W}_1 \cap \{p = \text{const}\} = \{(p, \tau, \theta) \in \mathbb{DM}^3 : p = \text{const}, \tau > 0, \ |\theta| < \pi/6\}. \tag{4.2}$$

Note that on the boundary between two wedges, two eigenvalues are equal; for example, $\sigma_2 = \sigma_3 < \sigma_1$ on the boundary between $\mathcal{W}_1$ and $\mathcal{W}_2$. With the obvious modifications of notation, we regard the wedges $\mathcal{W}_n$ as subsets of the space of *strain-rate* eigenvalues as well. As with stresses, for φ in each of the wedges, the strain-rate eigenvalues have a specific ordering.

Given a constitutive manifold $\mathcal{M}(\phi)$, let us define its restrictions to the individual wedges to be

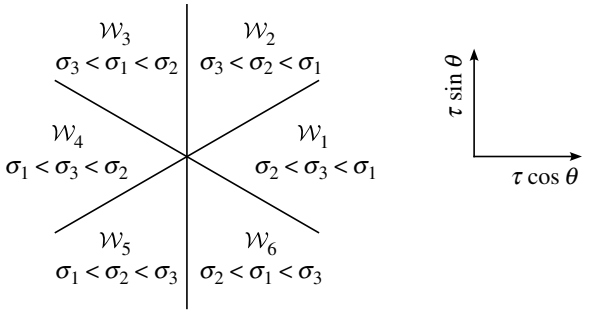

Figure 5. The six wedges $\mathcal{W}_n$ viewed in each subset $\{p = \text{const}\}$ of $\mathbb{DM}^3$.

$$\mathcal{M}_n(\phi) = \{(\boldsymbol{\sigma}, \boldsymbol{D}) \in \mathcal{M}(\phi) : \boldsymbol{D} \in \mathcal{W}_n\}, \qquad n = 1, 2, \ldots, 6. \tag{4.3}$$

The condition of isotropy implies that the constitutive relations are invariant under simultaneous permutations of σ_i and D_i, which can be seen by taking $\boldsymbol{R}$ in equation (2.2) to be the permutation matrices. Thus, a function $\boldsymbol{\sigma} = \Sigma(\boldsymbol{D}, \phi)$ initially defined on $\mathcal{W}_1$ extends, by isotropy, to be defined for all $\boldsymbol{D} \in \mathcal{W}_n$ ($n = 1, 2, \ldots, 6$). Since the union of all six $\mathcal{W}_n$ is dense in $\mathbb{DM}^3$, the full constitutive law is obtained by continuous extension, whenever possible. In other words, with isotropy, $\mathcal{M}_n(\phi)$ are determined by $\mathcal{M}_1(\phi)$, and

$$\mathcal{M}(\phi) = \bigcup_{n=1}^{6} \overline{\mathcal{M}_n}(\phi)\,. \tag{4.4}$$

The ordering principle (equation (2.5)) implies that if $\boldsymbol{D} \in \mathcal{W}_n$, then $\Sigma(\boldsymbol{D}, \phi)$ must belong to the same wedge $\mathcal{W}_n$; in symbols, $\mathcal{M}_n(\phi) \subset \mathcal{W}_n \times \mathcal{W}_n$. In terms of cylindrical coordinates, this means that θ and φ as related by a constitutive relation must be associated with the same wedge.

(b) The characteristic differential equations

Assuming the yield condition (equation (2.21)), for each value of ϕ, $\mathcal{M}(\phi)$ must be contained in the five-dimensional submanifold[4]

$$\mathcal{S}(\phi) = \{(p, \tau, \theta, q, s, \varphi) : \tau = p\, r(\theta, I, \phi),\ p \geq 0\} \subset \mathbb{DM}^3 \times \mathbb{DM}^3, \tag{4.5}$$

where $r(\theta, I, \phi)$ is the appropriate root of equation (2.20); note that we use cylindrical coordinates on both copies of $\mathbb{DM}^3$.

Our goal is to find $\mathcal{M}(\phi) \subset \mathcal{S}(\phi)$ that are Onsager symmetric and satisfy a few other properties. As shown in appendix A, the key to this lies in understanding solutions of the following system of ODEs, called the *characteristic equations*:[5,6]

$$\begin{aligned}
&\text{(a)} \quad \frac{\mathrm{d}p}{\mathrm{d}s} = 0,\\
&\text{(b)} \quad \frac{\mathrm{d}\theta}{\mathrm{d}s} = -\frac{\sin(\theta - \varphi)}{s\Delta(\theta, \varphi)},\\
&\text{(c)} \quad \frac{\mathrm{d}q}{\mathrm{d}s} = \frac{r(\theta, I)}{\Delta(\theta, \varphi)},\\
&\text{(d)} \quad \frac{\mathrm{d}\varphi}{\mathrm{d}s} = \frac{\sin(\theta - \varphi) - G(\theta)\cos(\theta - \varphi)}{s\Delta(\theta, \varphi)},
\end{aligned} \tag{4.6}$$

where G is defined in terms of the solution of equation (2.20):

$$G(\theta) = \frac{\hat{r}'(\theta)}{\hat{r}(\theta)} = -\frac{3\beta\hat{r}(\theta)\cos(3\theta)}{3\beta\hat{r}(\theta)\sin(3\theta) + 2}, \tag{4.7}$$

wherein

$$\Delta(\theta,\varphi)=\cos(\theta-\varphi)+G(\theta)\sin(\theta-\varphi). \tag{4.8}$$

In equations (4.6)–(4.8), the volume fraction ϕ is treated as a parameter, and for brevity, its appearance is suppressed; similarly below.

Remark 4.1. The characteristic equations (4.6) are obtained from Hamilton's equations for the Hamiltonian $H=pr(\theta,I)-\tau$ (see appendix A). Regularity of these equations for $s>0$ is provided by the following two facts: (a) In $G(\theta)$ the denominator $3\beta\hat{r}(\theta)\sin(3\theta)+2$ is positive (lemma B.1); (b) If θ,φ belong to the same wedge $\mathcal{W}_i$, then $\Delta(\theta,\varphi)>0$ (lemma A.1).

To explain the relation between $\mathcal{M}(\phi)$ and the characteristic equations (4.6), suppose that[7] $(\underline{p},\underline{\theta},\underline{q},\underline{\varphi})(s)$ is a solution of equations (4.6). Let $\underline{\tau}(s)$ be defined by the formulae

$$\underline{\tau}=r(\underline{\theta},\underline{I})\underline{p}\,,\quad \text{where}\quad \underline{I}(s)=\frac{2ds}{\sqrt{\underline{p}/\rho_*}}\,.$$

Then let $\underline{\sigma}(s)=(\underline{p},\underline{\tau},\underline{\theta})(s)$ and $\underline{D}(s)=(\underline{q}(s),s,\underline{\varphi}(s))$; it is clear from the definition of $\underline{\tau}$ that, as s varies,

$$(\underline{\sigma},\underline{D})(s) \tag{4.9}$$

traces out a curve in $\mathcal{S}(\phi)$, what we call a *characteristic curve*.

These characteristic curves are the building blocks of $\mathcal{M}(\phi)$. As we show in appendix A (see proposition A.1), if one point on a characteristic curve belongs to $\mathcal{M}(\phi)$, then the entire curve is contained in $\mathcal{M}(\phi)$; in symbols, if $\underline{\sigma}(s_0)=\Sigma(\underline{D}(s_0))$ for some s_0, then for all s,

$$\underline{\sigma}(s)=\Sigma(\underline{D}(s)); \tag{4.10}$$

moreover, $\mathcal{M}(\phi)$ is a union of such curves.

Remark 4.2. Figure 6 shows the projection into the q,s-subspace of a characteristic curve that passes through a strain rate $D_\star=(0,s_\star,0)$ describing simple shear; it terminates at a pure compression i.e. at a point where $s=0$ and $q<0$. Although τ,θ,φ vary along the curve, the pressure does not. This fact suggests an interpretation of these curves: they specify a trade-off between shearing and compression that leaves the pressure unchanged.

(c) The φ,θ-subsystem: behaviour as $s\longrightarrow 0$ and $s\longrightarrow\infty$

In equations (4.6), the φ- and θ-equations form a separate subsystem, which is singular as $s\to 0$. To handle this singularity, it is useful to change the independent variable by defining

$$\tilde{s}=\ln s, \tag{4.11}$$

so that $s=0$ corresponds to the limit as $\tilde{s}$ tends to $-\infty$. The resulting transformed equations are autonomous:

$$\begin{aligned}\frac{\mathrm{d}\tilde{\varphi}}{\mathrm{d}\tilde{s}}&=\frac{\sin(\tilde{\theta}-\tilde{\varphi})-G(\tilde{\theta})\cos(\tilde{\theta}-\tilde{\varphi})}{\Delta(\tilde{\theta},\tilde{\varphi})},\\ \frac{\mathrm{d}\tilde{\theta}}{\mathrm{d}\tilde{s}}&=-\frac{\sin(\tilde{\theta}-\tilde{\varphi})}{\Delta(\tilde{\theta},\tilde{\varphi})}\,.\end{aligned} \tag{4.12}$$

Now, since $\Delta(\tilde{\theta},\tilde{\varphi})>0$, one can rescale $\tilde{s}$ and consider instead the simpler equations below, for which we use the same notations as in equations (4.12):

$$\begin{aligned}\frac{\mathrm{d}\tilde{\varphi}}{\mathrm{d}\tilde{s}}&=\sin(\tilde{\theta}-\tilde{\varphi})-G(\tilde{\theta})\cos(\tilde{\theta}-\tilde{\varphi}),\\ \frac{\mathrm{d}\tilde{\theta}}{\mathrm{d}\tilde{s}}&=-\sin(\tilde{\theta}-\tilde{\varphi})\,.\end{aligned} \tag{4.13}$$

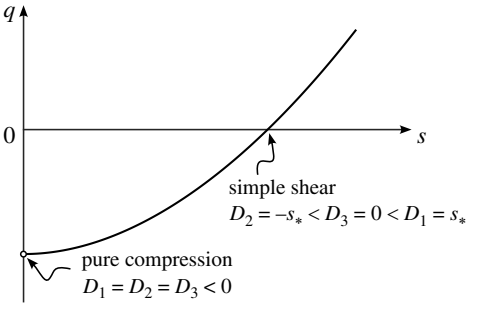

Figure 6. Projection of a characteristic curve that connects a simple shear deformation $(0, s_\star, 0)$ to pure compression.

Figure 7 shows the phase-plane portrait of equations (4.13) in the square $\{|\varphi|, |\theta| \le \pi/6\}$. We note the following properties:

— Equations (4.13) have two equilibria in $\{|\varphi|, |\theta| \le \pi/6\}$, namely, $E_- = (-\pi/6, -\pi/6)$ (a saddle) and $E_+ = (\pi/6, \pi/6)$ (a sink), which we show below.

— The unstable manifold emanates from the saddle E_- and asymptotes to the sink E_+ as $s \to \infty$. This trajectory lies below the diagonal $\{\theta = \varphi\}$.

In appendix A(c), we argue that the physically relevant characteristic curves in $\overline{\mathcal{M}_1}$ are defined for all $s > 0$ and their projections on to φ, θ are either one of the two equilibrium solutions $(\underline{\varphi}, \underline{\theta})(s) \equiv (\pm\pi/6, \pm\pi/6)$ of equations (4.6) or they trace out the unstable manifold as s varies from 0 to ∞. (Note that there are many different solutions $\{(\underline{\varphi}, \underline{\theta})(s)\}$ that map into this trajectory, resulting from the invariance of equation (4.13) under the translation $\tilde{s} \mapsto \tilde{s} + c$ for any $c \in \mathbb{R}$.)

To conclude the analysis of the φ, θ-subsystem, we verify that the equilibria E_- and E_+ of equations (4.13) are, respectively, a saddle and a sink, as claimed above. The Jacobians at E_- and E_+ are, respectively,

$$J_- = \begin{bmatrix} -1 & J_{12}^- \\ 1 & -1 \end{bmatrix}, \quad J_+ = \begin{bmatrix} -1 & J_{12}^+ \\ 1 & -1 \end{bmatrix} \tag{4.14}$$

where

$$J_{12}^\pm = 1 - G'(\pm\pi/6). \tag{4.15}$$

Both J_- and J_+ have negative trace; moreover,

$$\begin{aligned} \det J_- &= G'(-\pi/6) = \frac{9\beta\hat{r}(-\pi/6)}{3\beta\hat{r}(-\pi/6) - 2} < 0, \\ \det J_+ &= G'(\pi/6) = \frac{9\beta\hat{r}(\pi/6)}{3\beta\hat{r}(\pi/6) + 2} > 0, \end{aligned} \tag{4.16}$$

where both inequalities follow from lemma B.1. This verifies that E_- is a saddle and E_+ a sink. Also note that

$$\left(\sqrt{J_{12}^-}, 1\right) \tag{4.17}$$

is an eigenvector of J_- with the eigenvalue $\sqrt{J_{12}^-} - 1 > 0$. This eigenvector is tangent to the unstable manifold at E_-.

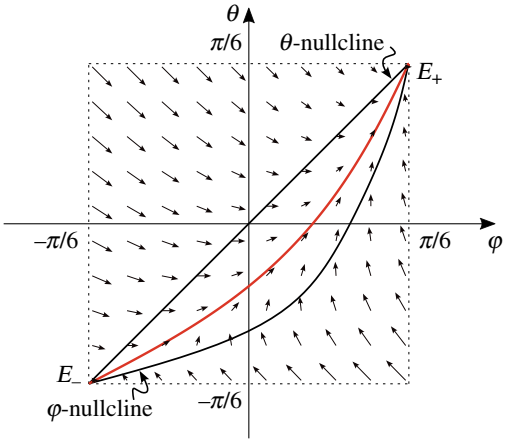

Figure 7. Phase diagram of equations (4.13) for $\phi = 0.56$, which corresponds to $(\beta, Y) = (0.610, 0.183)$ via equations (2.24) and (2.25) and the parameters listed in table 1. The red curve is the unstable manifold emanating from E_-.

(d) Calculation of the constitutive laws

(i) Overview

As noted in §4a, to determine the constitutive manifold $\mathcal{M}$, it suffices to focus on $\mathcal{M}_1$, the graph of the restriction of Σ to $\mathcal{W}_1$. To set the notation: given a point $D_\star = (q_\star, s_\star, \varphi_\star)$, we seek $\sigma_\star = \Sigma(D_\star) = (p_\star, \tau_\star, \theta_\star)$. For the time being, we assume $s_\star > 0$ and $|\varphi_\star| < \pi/6$; we deal with the boundary cases at the end of the section.

As we have stated above, $\mathcal{M}_1$ is a union of characteristic curves; the projections of these curves on to the (φ, θ)-plane emanate from the equilibrium E_- of equations (4.13) and follow the unstable manifold through the points $(\varphi_\star, \theta_\star)$. Thus, for the determination of $\sigma_\star$, we need one of these characteristic curves

$$(\underline{\sigma}, \underline{D})(s), \quad 0 < s \le s_\star \tag{4.18}$$

that satisfies the boundary conditions

$$\underline{q}(s_\star) = q_\star, \quad \underline{\varphi}(s_\star) = \varphi_\star\,. \tag{4.19}$$

In fact, these boundary conditions alone do not determine the curve uniquely (see proposition 4.1), but as we will see in §4a(iv) and §4a(v), we do obtain a unique characteristic curve when $\Phi(I)$-rheology is imposed. Once the appropriate characteristic $(\underline{\sigma}, \underline{D})(s)$ has been found, the stress $\sigma_\star$ is given by

$$\Sigma(D_\star) = \underline{\sigma}(s_\star)\,. \tag{4.20}$$

(ii) The Lode angle $\Theta(D_\star, \phi)$

Let us argue that $\theta_\star = \Theta(D_\star)$ is independent of $q_\star$ and $s_\star$. Restricting equations (4.19) to the φ, θ-subsystem of equations (4.6), we seek a solution $(\underline{\varphi}, \underline{\theta})(s) (0 \le s \le s_\star)$ with

$$\lim_{s \to 0^+} (\underline{\varphi}, \underline{\theta})(s) = (-\pi/6, -\pi/6), \quad \text{and} \quad \underline{\varphi}(s_\star) = \varphi_\star\,. \tag{4.21}$$

Such a solution follows the unstable manifold of equations (4.13) through E_-. Thus, $\theta_\star$ is just the θ-coordinate of the point where the unstable manifold, illustrated in figure 7, crosses the vertical line $\varphi = \varphi_\star$. We claim that such a point is unique; in appendix D, we show that

$\mathrm{d}\varphi/\mathrm{d}\theta > 0$ along the unstable manifold, which confirms the claim. Since the unstable manifold is independent of $q_\star$ and $s_\star$, so is $\theta_\star$. Accordingly, we write $\theta_\star = \Theta(\varphi_\star)$.

In the language of §4a(i), we may choose a solution $(\underline{\varphi}, \underline{\theta})(s)$ of the φ, θ-subsystem that parametrizes the unstable manifold and satisfies

$$\underline{\theta}(s_\star) = \Theta(\varphi_\star), \qquad \underline{\varphi}(s_\star) = \varphi_\star\,. \tag{4.22}$$

In appendix C, we derive a polynomial approximation of $\Theta(\varphi_\star)$.

Remark 4.3. To compute Θ directly, note that by eliminating s from the θ, φ-equations in equations (4.6), one obtains the ODE

$$\frac{\mathrm{d}\theta}{\mathrm{d}\varphi} = -\frac{\sin(\theta-\varphi)}{\sin(\theta-\varphi) - G(\theta)\cos(\theta-\varphi)}\,. \tag{4.23}$$

Let $\theta^{\mathrm{dir}}(\varphi)\,(\varphi \geq -\pi/6)$ ('dir' is mnemonic for 'direct') be the solution of equation (4.23) that satisfies the initial conditions[8]

$$\theta^{\mathrm{dir}}(-\pi/6) = -\pi/6, \qquad \frac{\mathrm{d}\theta^{\mathrm{dir}}}{\mathrm{d}\varphi}(-\pi/6) = \frac{1}{\sqrt{J_{12}}}\,. \tag{4.24}$$

Then $\Theta(\varphi)$ is just $\theta^{\mathrm{dir}}(\varphi)$.

(iii) Solution of the q-equation

Although the boundary conditions (equations (4.19)) are sufficient to determine the Lode angle $\theta_\star$, as the following proposition shows, they are not sufficient to determine the pressure $p_\star$. In the proposition, we use the function

$$Z(\varphi) = \frac{1}{2}\hat{r}(\Theta(\varphi))\cos\left[\Theta(\varphi) - \varphi\right] \tag{4.25}$$

defined in §3. Let $(\underline{\theta}, \underline{\varphi})(s)$ be a solution of the θ, φ-subsystem that satisfies equations (4.22).

Proposition 4.1. *For any positive constant* Γ, *if*

$$\text{(a) } \underline{p}(s) = \frac{4\rho_* d^2}{\Psi^2}\Gamma, \qquad \text{(b) } \underline{q}(s) = \frac{1}{\sqrt{\Gamma}}\left[Z(\underline{\varphi}(s))s^2 - Z(\underline{\varphi}(s_\star))s_\star^2\right] + q_\star, \tag{4.26}$$

then $(\underline{p}, \underline{\theta}, \underline{q}, \underline{\varphi})(s)$ *is a solution of equations (4.6) that satisfies equations (4.19).*

Remark 4.4. *The constant* Γ *may be interpreted as the pressure scaled by a factor that gives it the units of rate squared.*

Proof. We claim that if $\underline{p}$ is given by equation (4.26a), then

$$\underline{q}(s) = \frac{1}{\sqrt{\Gamma}}\left[Z(\underline{\varphi}(s))s^2 + K\right], \tag{4.27}$$

where K is an arbitrary constant, is the general solution of equation (4.6c). To see this, note that $\underline{\theta}(s) = \Theta(\underline{\varphi}(s))$, so

$$\frac{d}{ds}\Theta(\underline{\varphi}(s)) = \underline{\theta}'(s)\,.$$

A direct computation yields

$$\begin{aligned}\frac{d}{ds}[Z(\underline{\varphi}(s))s^2] = s\hat{r}(\underline{\theta})\cos(\underline{\theta}-\underline{\varphi}) + \frac{1}{2}s^2\hat{r}'(\underline{\theta})\underline{\theta}'\cos(\underline{\theta}-\underline{\varphi})\\ -\frac{1}{2}s^2\hat{r}(\underline{\theta})(\underline{\theta}'-\underline{\varphi}')\sin(\underline{\theta}-\underline{\varphi});\end{aligned} \tag{4.28}$$

in the right-hand side of this formula, we omit the argument s for $\underline{\theta}, \underline{\varphi}$ and their derivatives. By applying the identity $\hat{r}'(\underline{\theta}) = \hat{r}(\underline{\theta})G(\underline{\theta})$ equation (4.7) and equations (4.6b,d) to (4.28), we derive

$$\frac{d}{ds}[Z(\underline{\varphi}(s))s^2] = \frac{s\hat{r}(\underline{\theta})}{\Delta(\underline{\theta}, \underline{\varphi})}. \tag{4.29}$$

Thus, if $\underline{q}$ is given by equation (4.27), then

$$\frac{d}{ds}\underline{q}(s) = \frac{s}{\sqrt{\Gamma}}\frac{\hat{r}(\underline{\theta})}{\Delta(\underline{\theta}, \underline{\varphi})} = \frac{I}{\Psi}\frac{\hat{r}(\underline{\theta})}{\Delta(\underline{\theta}, \underline{\varphi})} = \frac{r(\underline{\theta}, \underline{I})}{\Delta(\underline{\theta}, \underline{\varphi})}, \tag{4.30}$$

where the last step follows from equation (2.22). This verifies the claim. The proof is completed by observing that equations (4.19) determine the constant K and yields equation (4.26b). ∎

(iv) Application of $\Phi(I)$-rheology

In case of simple shear $D_\dagger = (0, s_\dagger, 0)$, the pressure along the characteristic through $D_\dagger$ is determined by $\Phi(I)$-rheology equation (2.15); in this case, equations (4.26) become

$$\text{(a) } \underline{p}(s) = \frac{4\rho_* d^2}{\Psi^2}s_\dagger^2, \qquad \text{(b) } \underline{q}(s) = \frac{1}{s_\dagger}\left[Z(\underline{\varphi}(s))s^2 - Z(0)s_\dagger^2\right]. \tag{4.31}$$

It is useful to follow such a characteristic to the volumetric axis, by which we mean $\{s = 0\}$ in strain-rate space. Here all three strain-rate eigenvalues are equal, specifically equal to $\operatorname{div}\mathbf{u}/3$. According to equations (4.31), $q(0) = -Z(0)s_\dagger$. It follows that along the compressive part of the volumetric axis,[9] i.e.

$$\{D = (q, 0, \cdot) : q \le 0\}, \tag{4.32}$$

the pressure in $\Sigma(D)$ is given by

$$p = \frac{4\rho_* d^2}{\Psi^2 Z(0)^2}q^2. \tag{4.33}$$

Alternatively, in the manifold $\mathcal{M}_1$, the variable q along this axis may be expressed in terms of the scaled pressure Γ as in equations (4.26),

$$q = -Z(0)\sqrt{\Gamma}. \tag{4.34}$$

(v) Calculation of the pressure $P(D_\star, \phi)$

Now the characteristic derived from equations (4.26) meets the volumetric axis at

$$\underline{q}(0) = -\frac{1}{\sqrt{\Gamma}}Z(\underline{\varphi}(s_\star))s_\star^2 + q_\star. \tag{4.35}$$

But equation (4.34) expresses q along this axis in terms of the scaled pressure Γ, so we must have

$$-Z(0)\sqrt{\Gamma} = -\frac{1}{\sqrt{\Gamma}}Z(\underline{\varphi}(s_\star))s_\star^2 + q_\star. \tag{4.36}$$

This may be rewritten as a quadratic equation for $\sqrt{\Gamma}$ for which the positive solution is

$$\sqrt{\Gamma} = \frac{-q_\star + \sqrt{q_\star^2 + 4Z(0)Z(\varphi_\star)s_\star^2}}{2Z(0)}. \tag{4.37}$$

Squaring and undoing the scaling $p_\star = [4\rho_* d^2/Z(0)^2\Psi^2]\Gamma$, we obtain the constitutive equation

$$p_\star = \rho_* d^2 \left[\frac{\sqrt{q_\star^2 + 4Z(0,\phi)Z(\varphi_\star,\phi)s_\star^2} - q_\star}{\Psi(\phi)Z(0,\phi)} \right]^2 \tag{4.38}$$

of §3.

Of course, for the shear stress we have

$$\tau_\star = r(\theta_\star, I_\star)p_\star. \tag{4.39}$$

Remark 4.5. (i) It is easy to see that equation (4.38) reduces to equation (2.15) in simple shear, that is, when $q_\star = \varphi_\star = 0$. (ii) Note that equation (4.38) bears a striking similarity to the two-dimensional result (equation (3.5)).

(vi) Boundary cases

Up to this point we have assumed $s_\star > 0$ and $|\varphi_\star| < \pi/6$. We claim that equation (4.38) continues to be valid even if these assumptions do not hold. If $s_\star = 0$, then equation (4.38) predicts that $p_\star$ is zero if $q_\star > 0$ and is given by equation (4.33) if $q_\star < 0$, as desired. If $\varphi_\star = \pm\pi/6$, then $\underline{\theta}(s) \equiv \underline{\varphi}(s) \equiv \pm\pi/6$, and it may be checked that the various formulas above continue to be valid and justify equation (4.38).

5. Discussion and conclusions

A key result in this paper is to demonstrate some of the power of Onsager symmetry in the context of viscoplastic modelling: complete, dynamic three-dimensional constitutive laws may be derived from a three-dimensional yield condition and certain inputs from measurements of planar flow *provided* that Onsager symmetry is invoked. The result generates some interesting mathematics—in three-dimensions, the combination of a yield condition with Onsager symmetry yields an over-determined system of four algebro-differential equations for the stress eigenvalues as functions of the strain-rate eigenvalues. Here we demonstrate that a unique consistent solution can be formed by matching certain two-dimensional empirical data.

To illustrate this novel result, we introduce a rate-dependent yield condition analogous to the Lade–Duncan or Matsuoka–Nakai yield conditions, suitable to the inertial flow regime of granular material. We then derive the associated constitutive laws for this yield condition. This simple example agrees remarkably well with the DEM simulations of Clemmer *et al*. [17] that begin the study of flow beyond simple shear. Other constitutive laws, for both dry granular materials and suspensions, which follow [36], are derived from various yield conditions in electronic supplementary material II.

Although we have defined and studied Onsager symmetry independently of dissipation potentials, the usual derivation of the symmetry is based on such potentials. In the electronic supplementary material, we also show that our constitutive law may in fact be derived as the gradient of a convex dissipation potential.

Many complexities of three-dimensional flow remain uninvestigated. Steady simple shear—divergence-free flow with one strain-rate eigenvalue vanishing—has been the primary focus of both experiments and simulations. The pioneering work of Clemmer *et al*. [17] broke out of this context by studying steady, divergence-free flow with all three strain-rate eigenvalues, and hence the strain-rate Lode angle, non-zero. The present paper derives constitutive laws that apply for all strain rates and allow for dynamical behaviour.

Much additional work will be required to test such predictions in these new unexplored regimes. In addition to different geometries, dynamical problems will need to be studied as is illustrated by the following observation: the usual two-dimensional version of $\mu(I), \Phi(I)$ rheology [9,11] may be summarized by the equations

$$|\tau| = \mu(I)p, \quad I = \Psi(\phi),$$

but as far as steady flow is concerned, these equations cannot not be distinguished from

$$|\tau| = \mu(\Psi(\phi))p, \quad I = \Psi(\phi).$$

However, the two theories will predict different dynamical behaviour. Similar considerations apply to our newly proposed three-dimensional yield condition, and hence the full three-dimensional constitutive equations which result from it.

Another important task will be to establish criteria for well-posedness for these three-dimensional constitutive relations. In two-dimensional CIDR, it was shown in [12] that the dynamical equations are linearly well posed provided the underlying constitutive laws have Onsager symmetry and the two inequalities (2.20) of [12] are satisfied. The new constitutive laws derived here have Onsager symmetry and the three-dimensional analogues of (2.20) of [12] are satisfied. We therefore conjecture that the resulting dynamical equations are linearly well posed.

Data accessibility. Supplementary material is available online [37].

Declaration of AI use. We have not used AI-assisted technologies in creating this article.

Authors' contributions. Y.H.: conceptualization, formal analysis, investigation, methodology, project administration, validation, visualization, writing—original draft, writing—review and editing; D.G.S.: conceptualization, formal analysis, investigation, methodology, project administration, validation, writing—original draft, writing—review and editing; T.B.: conceptualization, data curation, formal analysis, funding acquisition, investigation, methodology, project administration, software, validation, visualization, writing—original draft, writing—review and editing.

All authors gave final approval for publication and agreed to be held accountable for the work performed therein.

Conflict of interest declaration. We declare we have no competing interests.

Funding. DGS & TB are grateful for support from the LMS and the Heilbronn institute, DGS is grateful for support under EPSRC grant EP/M022447/1, TB is grateful for the support of the NERC grants NE/R011001/1 and NE/W004240/1, and YH is grateful for support from CU Boulder, the China Postdoctoral Science Foundation (Grant 2021TQ0014), and Shanghai Jiao Tong University (Grant WH220407115).

Acknowledgements. We are grateful to Robert Bryant for directing our attention to the relevance of differential geometry for this problem and to Nico Gray for discussions that helped shape our thinking about the problem. We are also indebted to Joel Clemmer and Ishan Srivastava for kindly sharing their DEM data and enthusiasm for our pursuit; the American Physical Society also granted permission to use the data [17] for this open access publication.

Appendix A. Derivation of the characteristic equations

In §4b, we claimed that for each fixed ϕ the characteristic equations (equations (4.6)) are Hamilton's equations derived from the Hamiltonian

$$H = pr(\theta, I, \phi) - \tau\,. \tag{A 1}$$

In this appendix, we prove this claim and show that the flow of the characteristic equations is tangent to the constitutive manifold $\mathcal{M}(\phi)$, and hence $\mathcal{M}(\phi)$ is a union of characteristic curves. Since ϕ is held constant throughout the derivation, we suppress its notation, as we did for most of §4.

Given a Hamiltonian H, in *Cartesian* coordinates, Hamilton's equations are the ODEs

$$\dot{\sigma}_i = \frac{\partial H}{\partial D_i}, \quad \dot{D}_i = -\frac{\partial H}{\partial \sigma_i} \qquad (i = 1,2,3). \tag{A 2}$$

However, we want to work with cylindrical coordinates for stress (p, τ, θ) and strain rate (q, s, φ), which moreover are not conjugate to one another. To deal with the complications, as well as to prove the tangency result, it is most efficient to call on the language of differential geometry.

(a) Theoretical preparation

Recall that a constitutive manifold

$$\mathcal{M} = \{(\boldsymbol{\sigma}, \boldsymbol{D}) \in \mathbb{DM}^3 \times \mathbb{DM}^3 : \boldsymbol{\sigma} = \Sigma(\boldsymbol{D})\} \tag{A 3}$$

is Onsager symmetric if

$$\frac{\partial \Sigma_i}{\partial D_j} = \frac{\partial \Sigma_j}{\partial D_i}. \tag{A 4}$$

Introducing the following *symplectic 2-form* (cf. [38, p. 565]):

$$\omega = \sum_i \mathrm{d}\sigma_i \wedge \mathrm{d}D_i \tag{A 5}$$

on $\mathbb{DM}^3 \times \mathbb{DM}^3$, we claim that equation (A 4) holds if and only if the restriction of ω to (each tangent space of) $\mathcal{M}$ vanishes. This is easy to see, since substituting $\sigma_i = \Sigma_i(D)$ in equation (A 5) yields

$$\omega|_{\mathcal{M}} = \sum_i \mathrm{d}\Sigma_i \wedge \mathrm{d}D_i = \sum_{i,j} \frac{\partial \Sigma_i}{\partial D_j} \mathrm{d}D_j \wedge \mathrm{d}D_i = -\sum_{i<j} \left(\frac{\partial \Sigma_i}{\partial D_j} - \frac{\partial \Sigma_j}{\partial D_i} \right) \mathrm{d}D_i \wedge \mathrm{d}D_j, \tag{A 6}$$

and the two-forms $\{\mathrm{d}D_i \wedge \mathrm{d}D_j : i < j\}$ are linearly independent. Thus, we can use the condition

$$\omega|_{\mathcal{M}} = 0 \tag{A 7}$$

to characterize Onsager symmetry in terms of arbitrary coordinates. To invoke terminology from symplectic geometry, constitutive relations are Onsager symmetric if and only if the associated manifold $\mathcal{M}$ is *Lagrangian*.[10]

In light of the yield condition (equation (2.21)), we must seek a Lagrangian manifold $\mathcal{M}$ that is contained in the zero level set of H. On the other hand, H generates a Hamiltonian vector field X_H on $\mathbb{DM}^3 \times \mathbb{DM}^3$, which is invariantly defined as follows (cf. [38, p. 574]):

$$\omega(X_H, Y) = \mathrm{d}H(Y) \quad \text{for any vector field } Y. \tag{A 8}$$

Moreover, X_H is tangent to each level set of H, and its flow is just Hamilton's equations (see [38, proposition 22.16]). See equation (A 15) for an interpretation of this formula in coordinates.

The following proposition, an immediate consequence of the Hamiltonian flowout theorem in symplectic geometry (see [38, theorem 22.23]), shows that $\mathcal{M}$ is tangent to X_H; thus, $\mathcal{M}$ is a union of a two-parameter family of integral curves of X_H, what we call characteristic curves. Here, we include a proof of the proposition.

Proposition A.1. *If $\mathcal{M}$ is a Lagrangian submanifold of $\mathbb{DM}^3 \times \mathbb{DM}^3$ that is contained in the level set $H^{-1}(0)$, then for any $\boldsymbol{p} \in \mathcal{M}$, the Hamiltonian vector field X_H is tangent to $\mathcal{M}$ at $\boldsymbol{p}$.*

Proof. Suppose X_H were not tangent to $\mathcal{M}$ at some $\boldsymbol{p} \in \mathcal{M}$. As a result, the tangent space $T_{\boldsymbol{p}}\mathcal{M}$ and the vector $X_H(\boldsymbol{p})$ span a four-dimensional linear subspace $\mathcal{V}$ of $\mathbb{DM}^3 \times \mathbb{DM}^3$. We claim that

$$\omega(\boldsymbol{v}_1, \boldsymbol{v}_2) = 0, \qquad \forall \boldsymbol{v}_1, \boldsymbol{v}_2 \in \mathcal{V}. \tag{A 9}$$

To prove this claim, write $\boldsymbol{v}_i = \boldsymbol{w}_i + a_i X_H (i = 1,2)$ with $\boldsymbol{w}_i \in T_{\boldsymbol{p}}\mathcal{M}$ and $a_i \in \mathbb{R}$. Thus,

$$\omega(\boldsymbol{v}_1, \boldsymbol{v}_2) = \omega(\boldsymbol{w}_1, \boldsymbol{w}_2) + a_1\omega(X_H, \boldsymbol{w}_2) + a_2\omega(\boldsymbol{w}_1, X_H) + a_1 a_2\, \omega(X_H, X_H).$$

The first term $\omega(\boldsymbol{w}_1, \boldsymbol{w}_2)$ vanishes because $\mathcal{M}$ is Lagrangian; by equation (A 8), $\omega(X_H, \boldsymbol{w}_2) = \mathrm{d}H(\boldsymbol{w}_2)$, which vanishes because $\boldsymbol{w}_2$ is tangent to $\mathcal{M} \subset H^{-1}(0)$; $\omega(\boldsymbol{w}_1, X_H)$ vanishes for a similar reason; the last term vanishes by the skew symmetry of ω. This proves the claim.

Since the claim violates the standard fact that ω cannot vanish on a subspace of dimension greater than $3 = \frac{1}{2} \times 6$ (see [38, proposition 22.5]), we get a contradiction.

(b) The calculation

By substituting equation (2.7) in equation (A 5), the symplectic form ω is expressed in terms of the cylindrical coordinates $(p, \tau, \theta, q, s, \varphi)$:

$$\omega = -\mathrm{d}p \wedge \mathrm{d}q + 2a\,\mathrm{d}\tau \wedge \mathrm{d}s + 2bs\,\mathrm{d}\tau \wedge \mathrm{d}\varphi - 2b\tau\,\mathrm{d}\theta \wedge \mathrm{d}s + 2a\tau s\,\mathrm{d}\theta \wedge \mathrm{d}\varphi, \tag{A 10}$$

where to shorten formulas, we write $a = \cos(\theta - \varphi)$, $b = \sin(\theta - \varphi)$.
Defining $(x_1, \ldots, x_6) = (p, \tau, \theta, q, s, \varphi)$, we rewrite equation (A 10) as

$$\omega = \frac{1}{2}\sum_{i,j=1}^{6} \omega_{ij}\mathrm{d}x_i \wedge \mathrm{d}x_j, \tag{A 11}$$

where ω_{ij} enumerate the entries of the skew-symmetric matrix

$$W = \begin{bmatrix} 0 & 0 & 0 & -1 & 0 & 0 \\ 0 & 0 & 0 & 0 & 2a & 2sb \\ 0 & 0 & 0 & 0 & -2\tau b & 2\tau sa \\ 1 & 0 & 0 & 0 & 0 & 0 \\ 0 & -2a & 2\tau b & 0 & 0 & 0 \\ 0 & -2sb & -2\tau sa & 0 & 0 & 0 \end{bmatrix}. \tag{A 12}$$

By (A 8), the Hamiltonian vector field X_H is defined by the equations

$$\omega(X_H, \partial_j) = \partial_j H \qquad (j = 1, 2, \ldots, 6). \tag{A 13}$$

Writing $X_H = \sum_i \xi_i \partial_i$ and noting that $\omega(\partial_i, \partial_j) = \omega_{ij}$, the left-hand side of equation (A 13) is just

$$\omega(X_H, \partial_j) = \sum_i \xi_i \omega_{ij} = -\sum_i \omega_{ji}\xi_i, \tag{A 14}$$

and thus equation (A 13) reduces to a system of linear equations

$$W\xi = -\nabla H, \tag{A 15}$$

where ξ denotes the column vector $(\xi_1, \xi_2, \ldots, \xi_6)$.
For simplicity, let us write $\lambda = 2d\sqrt{\rho_*}$. Thus, $I = \lambda s/\sqrt{p}$, and

$$\nabla H = \begin{bmatrix} r - \dfrac{I}{2}\partial_I r \\ -1 \\ p\,\partial_\theta r \\ 0 \\ \lambda\sqrt{p}\,\partial_I r \\ 0 \end{bmatrix}. \tag{A 16}$$

On solving equation (A 15), we obtain

$$\xi = \begin{bmatrix} 0 \\ \dfrac{\lambda a}{2}\sqrt{p}\partial_I r \\ -\dfrac{\lambda b}{2\tau}\sqrt{p}\partial_I r \\ r - \dfrac{I}{2}\partial_I r \\ \frac{1}{2}\left(a + \frac{bp}{\tau}\partial_\theta r\right) \\ \frac{1}{2s}\left(b - \frac{ap}{\tau}\partial_\theta r\right) \end{bmatrix}. \tag{A 17}$$

royalsocietypublishing.org/journal/rspa Proc. R. Soc. A 480: 20230955

$$\begin{bmatrix} p' \\ \tau' \\ \theta' \\ q' \\ s' \\ \varphi' \end{bmatrix} = \begin{bmatrix} 0 \\ \frac{\lambda a}{2}\sqrt{p}\,\partial_I r \\ -\frac{\lambda b}{2\tau}\sqrt{p}\,\partial_I r \\ r - \frac{I}{2}\partial_I r \\ \frac{1}{2}\left(a + \frac{bp}{\tau}\partial_\theta r\right) \\ \frac{1}{2s}\left(b - \frac{ap}{\tau}\partial_\theta r\right) \end{bmatrix}, \tag{A 18}$$

define integral curves of the Hamiltonian vector field X_H. Since the five variables p, θ, q, s, φ provide coordinates for $\mathcal{S}(\phi)$, we may delete the τ-equation from equation (A 18), which follow from the relation $\tau = pr(\theta, I)$ and the equations for p, θ, s. Additionally, we substitute $\tau = pr(\theta, I)$ in the denominators of ξ_s and ξ_φ to simplify the s' and φ' equations. For example,

$$s' = \tfrac{1}{2}\left(a + \tfrac{bp}{\tau}\partial_\theta r\right) = \tfrac{1}{2}\left(a + \tfrac{b}{r}\partial_\theta r\right) = \tfrac{1}{2}\left(a + \tfrac{bp}{\hat{r}}\hat{r}'\right),$$

where $\hat{r} = \Psi r/I$, which depends on θ (and ϕ) but none of the other coordinates p, q, s, φ.
Now let us impose the yield condition (equation (2.16)):

$$\beta\hat{r}^3 \sin 3\theta + \hat{r}^2 = Y. \tag{A 19}$$

By differentiating equation (A 19), we obtain

$$\frac{\hat{r}'(\theta)}{\hat{r}(\theta)} = G(\theta) := -\frac{3\beta\hat{r}(\theta)\cos(3\theta)}{3\beta\hat{r}(\theta)\sin(3\theta) + 2}, \tag{A 20}$$

which justifies equation (4.7). Furthermore, since

$$\partial_I r = \frac{r}{I}, \qquad \text{we have} \qquad \frac{\lambda\sqrt{p}\,\partial_I r}{\tau} = \frac{1}{s}.$$

Using these, equation (A 18) simplifies:

$$\begin{aligned} p' &= 0, \\ \theta' &= -\sin(\theta - \varphi)/2s, \\ q' &= r/2, \\ s' &= [\cos(\theta - \varphi) + G(\theta)\sin(\theta - \varphi)]/2, \\ \varphi' &= [\sin(\theta - \varphi) - G(\theta)\cos(\theta - \varphi)]/2s. \end{aligned} \tag{A 21}$$

Finally, the following lemma allows us to introduce s as the independent variable and obtain equations (4.6).

Lemma A.1. *Provided θ and φ belong to the same wedge $\overline{\mathcal{W}_i}$, we have*

$$\Delta(\theta, \varphi) := \cos(\theta - \varphi) + G(\theta)\sin(\theta - \varphi) > 0. \tag{A 22}$$

Proof. We note that equations (A 21), and in particular $\Delta(\theta, \varphi)$, is invariant as one performs the following two types of transformations for θ, φ while holding the other variables fixed:

$$(\theta, \varphi) \mapsto (\theta + 2\pi/3, \varphi + 2\pi/3) \quad \text{and} \quad (\theta, \varphi) \mapsto (\pi - \theta, \pi - \varphi). \tag{A 23}$$

Thus, it suffices to prove equation (A 22) under the assumption $|\theta|, |\varphi| \le \pi/6$. For such θ and φ, $\cos(\theta - \varphi)$ is always positive. Since $G(\pm\pi/6) = 0$, we have $\Delta(\pm\pi/6, \varphi) > 0$ for $\varphi \in [-\pi/6, \pi/6]$. To proceed, assume $\theta \in (-\pi/6, \pi/6)$, and we rewrite equation (4.8) as

$$\Delta(\theta, \varphi) = \cos(\theta - \varphi)G(\theta)\left[\tan(\theta - \varphi) + \frac{1}{G(\theta)}\right]. \tag{A 24}$$

In equation (A 24), $\cos(\theta-\varphi)>0$ as mentioned above; $G(\theta)<0$ owing to equation (4.7) and lemma B.1. Thus, it remains to prove that $\tan(\theta-\varphi)+1/G(\theta)<0$. Let us write

$$\frac{1}{G(\theta)} = -\left(\tan 3\theta + \frac{2}{3\beta\hat{r}(\theta)\cos 3\theta}\right).$$

Because $\hat{r}(\theta)$ attains maximum value at $\theta=-\pi/6$ (according to equation (4.7)), lemma B.1 implies that $2/(3\beta\hat{r}(\theta))\geq 1$; consequently,

$$\frac{1}{G(\theta)} \leq -\left(\tan 3\theta + \frac{1}{\cos 3\theta}\right) = -\tan\left(\frac{3}{2}\theta+\frac{\pi}{4}\right),$$

and therefore

$$\tan(\theta-\varphi)+\frac{1}{G(\theta)} \leq \tan(\theta-\varphi)-\tan\left(\frac{3}{2}\theta+\frac{\pi}{4}\right),$$

the right-hand side of which is negative, since $\theta-\varphi<(3/2)\theta+\pi/4$ for $\theta\in(-\pi/6,\pi/6)$ and $\varphi\in[-\pi/6,\pi/6]$. This completes the proof.

(c) Admissible characteristics

We now justify a characterization from §4c of the physically relevant characteristic curves contained in $\overline{\mathcal{M}_1}$. The argument is based on the observation that any characteristic curve contained in $\overline{\mathcal{M}_1}$ belongs to one of the following three cases.

Case 1. $\underline{\theta}(s)=\underline{\varphi}(s)=\pm\pi/6$ *somewhere along the curve*. In this case, the entire curve collapses on to one of the equilibria of equations (4.13), giving rise to the two trivial cases in the characterization of solutions.

Case 2. The curve meets the boundary of $\overline{\mathcal{W}_1}\times\overline{\mathcal{W}_1}$ *without belonging to Case 1*. In other words, along the curve there exists a point P where $|\theta|=\pi/6$ and $|\varphi|<\pi/6$, or vice versa. Without loss of generality, let us assume that $\theta=\pi/6$ and $|\varphi|<\pi/6$ at P. Using P as the initial condition for equations (4.6), we can extend the curve farther. Since $\mathrm{d}\theta/\mathrm{d}s\neq 0$ at P, along the extended curve there exists a point P', also belonging to $\mathcal{M}$, at which $\theta>\pi/6$ and $|\varphi|<\pi/6$ i.e. $P'\in\mathcal{W}_2\times\mathcal{W}_1$. This contradicts the ordering principle. Therefore, case 2 cannot occur.

Case 3. The curve is contained in the interior of $\overline{\mathcal{W}_1}\times\overline{\mathcal{W}_1}$. In this case, let us assume that the curve, $(\sigma,D)(s)$, is defined on a maximally extended open interval (s_1,s_2) with the possibility that $s_2=\infty$. For the sake of deriving a contradiction, suppose that $s_1>0$. Then the right-hand side of equations (4.6) are uniformly bounded for all s close to s_1; as a result, the denominators in equation (4.5) are bounded away from zero so the limit $Q=\lim_{s\to s_1^+}(\sigma,D)(s)$ exists. By cases 1 and 2, Q cannot belong to the boundary of $\overline{\mathcal{W}_1}\times\overline{\mathcal{W}_1}$, but by using Q as the initial condition of equations (4.6), the curve can be extended farther, contradicting maximality of the interval (s_1,s_2). Therefore, $s_1=0$. Using a similar argument, one shows that $s_2=\infty$. This proves that the curve is defined for all $s>0$. Any solution of equations (4.6) other than the unstable manifold would leave $\overline{\mathcal{W}_1}\times\overline{\mathcal{W}_1}$ at some finite, positive time, which completes the proof.

Appendix B. Properties of the three-dimensional yield surface

We recall equation (2.16):

$$\beta r^3\sin 3\theta + r^2 = Y, \tag{B 1}$$

which includes both the Lade–Duncan and Matsuoka–Nakai conditions. As we discuss below, parameters such that

$$\beta=\beta_0(Y) := \frac{2}{\sqrt{27}}\frac{1}{\sqrt{Y}} \tag{B 2}$$

are a limiting case for equation (B 1). This discussion also applies to equation (2.20) since the scaling of coefficients in equation (2.20) by powers of $I/\Psi(\phi)$ affects both sides of equation (B 2) equally.

If equation (B 2) is satisfied, the solution set of equation (B 1) consists of three straight lines, the line

$$r = -\frac{\sqrt{3}}{2\sin\theta}\sqrt{Y} \tag{B 3}$$

plus the lines obtained by rotating this one about the origin through $\pm 2\pi/3$ (figure 8*a*). In particular, we have the factorization

$$Y - r^2 - \beta_0(Y) r^3 \sin(3\theta) = Y \prod_{k=0}^{2} \left[\frac{2}{\sqrt{3}} \left(\frac{r}{\sqrt{Y}} \right) \sin\left(\theta + \frac{2k\pi}{3} \right) + 1 \right]. \tag{B 4}$$

Inside the (closed) triangle in the figure, $r \le \sqrt{3}\sqrt{Y}$, the maximum value occurring, for example, at $\theta = -\pi/6$, which corresponds to triaxial compression.

On the other hand, if $0 < \beta < \beta_0(Y)$, we have the following lemma.

Lemma B.1. *If $0 < \beta < \beta_0(Y)$, then the solution set of equation (B 1) has a unique bounded component in the r, θ-plane (see figure 8b), and points on this component satisfy $3\beta r \sin 3\theta + 2 > 0$.*

Proof. For each θ, the radius r of a point (r, θ) on the bounded component of the solution set of equation (B 1) is the smallest positive value of r that satisfies equation (B 1).

If $\sin 3\theta \ge 0$, then equation (B 1) has a unique positive solution and both terms of $3\beta r \sin 3\theta + 2$ are positive. If $\sin 3\theta < 0$, the left-hand side of (B 1) achieves the maximum $4/(27\beta^2 \sin^2 3\theta)$, for $r \ge 0$, at $r = -2/(3\beta \sin 3\theta)$. Thus, if $Y < 4/(27\beta^2)$, or equivalently $|\beta| < \beta_0(Y)$, then (B 1) has two positive roots, say $0 < r_1 < r_2$, and (θ, r_1) belongs to the bounded component of the solution set. Manifestly, at $r = r_1$ the slope of the function $\beta r^3 \sin 3\theta + r^2$ is positive, and hence $3\beta r_1 \sin 3\theta + 2 > 0$, which completes the proof.

Appendix C. Calculation of the yield functions from DEM data

Here, the method of fitting the ϕ-dependent constitutive functions using DEM data of simple shear flow is detailed. The steps will be illustrated using the data of Srivastava *et al*. [29]. First, the $I = \Psi(\phi)$ relation is fit against the proposed linear form equation (2.14) to identify ϕ_c and I_*. This is shown in the top panel of figure 1.

Fitting of the remaining yield functions $Y(\phi)$ and $\beta(\phi)$ is a little more involved because (for each ϕ) the two functions satisfy the two coupled equations

$$\Theta(0; Y, \beta) = \theta, \qquad \text{and} \qquad \beta \hat{r}^3 \sin(3\theta) + \hat{r}^2 = Y, \tag{C 1}$$

where θ and $\hat{r}$ are values measured in the DEM simulation at this value of ϕ. This task was simplified by considering the following expansion for Θ, which is also of general interest, rather than relying on numerical solutions of the ODE (equation (4.23)). Figure 9 shows that the approximation is quite accurate near $\varphi = 0$ where it is needed.

Claim C.1. $\Theta(\varphi, \phi)$ *has the expansion*

$$\Theta(\varphi, \phi) = -\pi/6 + \frac{1}{A}\hat{\varphi} - \frac{B}{A^4}\hat{\varphi}^3 + \mathcal{O}(\hat{\varphi}^5) \tag{C 2}$$

where $\hat{\varphi} = \varphi + \pi/6$ and A, B are determined as follows: let $\hat{r}_0 = \hat{r}(-\pi/6, \phi)$, define

$$\begin{aligned} G_1 &= G'(-\pi/6) = \frac{9\beta\hat{r}_0}{3\beta\hat{r}_0 - 2}, \\ G_3 &= \frac{1}{6}G'''(-\pi/6) = \frac{27\beta\hat{r}_0}{(3\beta\hat{r}_0 - 2)^3}(9\beta^2\hat{r}_0^2 - 6\beta\hat{r}_0 - 2), \end{aligned} \tag{C 3}$$

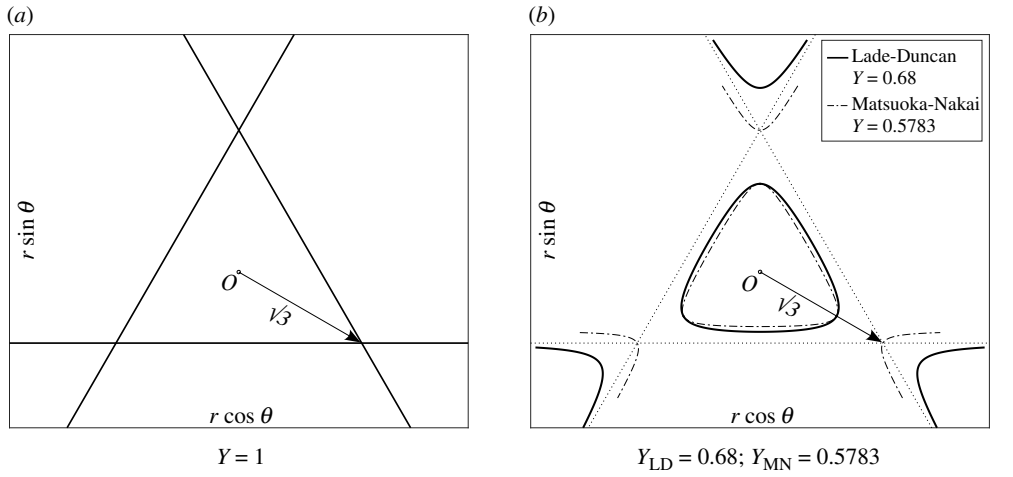

Figure 8. (*a*) Solution set of equation (2.20) when $Y = 1$ and $\beta = 2/\sqrt{27}$; (*b*) solution curves of Lade–Duncan (LD) and Matsuoka--Nakai (MN) yield equations for particular choices of Y and β given by equation (2.17).

and then let

$$A = \sqrt{1 - G_1},$$
$$B = -\frac{1}{6}\frac{G_1^2 + 2AG_1 - 2G_1 + 3G_3}{2A - 1}. \tag{C 4}$$

In particular, on comparing with equation (4.15), we have $A = \sqrt{J_{12}}$.

Proof. Write $\hat{\theta} = \theta + \pi/6$ and $\hat{\varphi} = \varphi + \pi/6$. In terms of $\hat{\theta}$ and $\hat{\varphi}$, equation (4.23) reads

$$\frac{\mathrm{d}\hat{\theta}}{\mathrm{d}\hat{\varphi}} = -\frac{\sin(\hat{\theta} - \hat{\varphi})}{\sin(\hat{\theta} - \hat{\varphi}) - G(\hat{\theta} - \pi/6)\cos(\hat{\theta} - \hat{\varphi})}. \tag{C 5}$$

Here $G(\hat{\theta} - \pi/6, \phi)$ is odd in $\hat{\theta}$, which has the expansion $G(\hat{\theta} - \pi/6, \phi) = G_1\hat{\theta} + G_3\hat{\theta}^3 + \mathcal{O}(\hat{\theta}^5)$ where G_1, G_3 are given by equation (C 3). By writing $\hat{\theta} = t_1\hat{\varphi} + t_3\hat{\varphi}^3 + \mathcal{O}(\hat{\varphi}^5)$, substituting it in equation (C 5), and expanding both sides of the resulting equation in powers of $\hat{\varphi}$, we obtain $t_1 = 1/A$ and $t_3 = -B/A^4$ upon comparing the coefficients, where A and B are given by equation (C 4).

Solutions of equations (C 1), using the approximation equation (C 2), are given as open circles in figure 1 with best fit parameters listed in table 1.

Appendix D. Slope of an unstable manifold

In §4d(ii), we claimed that $\mathrm{d}\varphi/\mathrm{d}\theta > 0$ along the unstable manifold of equations (4.13) that originates at E_-; this claim further implies that the function $\Theta(\varphi, \phi)$ exists and is strictly increasing in φ. Here we justify the claim.

The idea is to show that both the θ- and φ-nullclines have strictly positive slope (figure 7). Once this is verified, then along the boundary of the trapping region enclosed by the nullclines the flow of equations (4.13) point *inward*. Therefore, the unstable manifold must be contained in the trapping region, and its slope cannot change sign. Since the unstable manifold has positive slope at E_-, the claim is justified.

Now we verify that the θ- and φ-nullclines have positive slope. The former is a straight line with slope 1, so it remains to show that $\mathrm{d}\varphi/\mathrm{d}\theta > 0$ along the φ-nullcline.

The φ-nullcline is the graph of the function $\varphi(\theta) = \theta - \arctan(G(\theta))$. Direct calculation shows

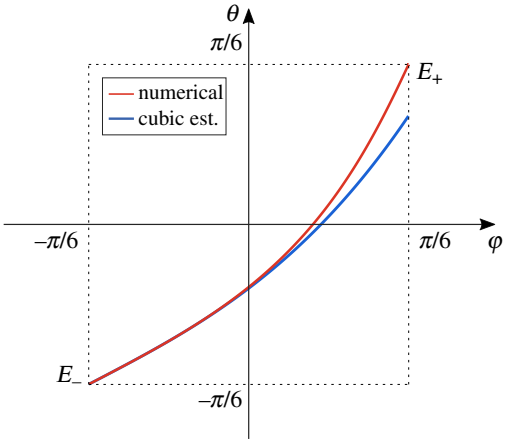

Figure 9. The graph of a numerical solution (in red) of equation (4.23) initiating at E_- and its cubic approximation using (C 2) (in blue) for $\phi = 0.56$, which corresponds to $(\beta, Y) = (0.610, 0.183)$ via equations (2.24) and (2.25) and the parameter values listed in table 1.

$$\varphi'(\theta) = 1 + \frac{-27\beta^2[\hat{r}(\theta)]^2 + 6\beta\hat{r}'(\theta)\cos 3\theta - 18\beta\hat{r}(\theta)\sin 3\theta}{9\beta^2[\hat{r}(\theta)]^2 + 12\beta\hat{r}(\theta)\sin 3\theta + 4}. \tag{D 1}$$

Hence, the condition $\varphi'(\theta) > 0$ is equivalent to

$$9\beta^2\hat{r}^2 + 12\beta\hat{r}\sin 3\theta + 4 > 27\beta^2\hat{r}^2 - 6\beta\hat{r}'\cos 3\theta + 18\beta\hat{r}\sin 3\theta, \tag{D 2}$$

which, by equation (4.7), is just

$$4 > 18\beta^2\hat{r}^2 + 6\beta\hat{r}\left(\sin 3\theta + \frac{3\beta\hat{r}\cos^2 3\theta}{3\beta\hat{r}\sin 3\theta + 2}\right). \tag{D 3}$$

By lemma B.1, $3\beta\hat{r}\sin 3\theta + 2 > 0$, so (D 3) reduces to the following in succession:

$$\begin{aligned} 2(3\beta\hat{r}\sin 3\theta + 2) &> 9\beta^2\hat{r}^2(3\beta\hat{r}\sin 3\theta + 2) + 9\beta^2\hat{r}^2 + 6\beta\hat{r}\sin 3\theta, \\ 4 &> 27\beta^3\hat{r}^3\sin 3\theta + 27\beta^2\hat{r}^2, \\ \frac{4}{27\beta^2} &> \beta\hat{r}^3\sin 3\theta + \hat{r}^2 = Y, \end{aligned} \tag{D 4}$$

where the last equality is just the yield equation equation (2.16) and the inequality $4/(27\beta^2) > Y$ follows from our assumption $\beta < \beta_0(Y)$ equation (2.19). This proves that $\mathrm{d}\varphi/\mathrm{d}\theta > 0$ along the φ-nullcline.

Endnotes

[1]A material obeying the constitutive law (equation (2.3)) is called a *Reiner–Rivlin* fluid [24, p. 478].

[2]Clemmer *et al*. [17] observed this ordering in all their simulations. In simple shear with $D_1 < D_2 = 0 < D_3$, the ordering principle means the largest stress (in absolute value) is associated with the compressive strain rate D_1; the smallest, with the expansive strain rate D_3; the intermediate stress with the vanishing strain rate D_2.

[3]See §4a for discussion of the full range of Lode angles.

[4]Strictly speaking, if $p = 0$ then $r(\theta, I)$ is undefined because $I \sim 1/\sqrt{p}$. However, it may be seen from equation (2.20) that $r \sim I \sim 1/\sqrt{p}$ as $p \to 0$, so $pr(\theta, I, \phi)$ is continuous in this limit. Incidentally, it turns out that in the constitutive law $p = 0$ if and only if $s = 0$ and $q \geq 0$ i.e. for pure expansion without shearing.

[5]A physical interpretation of the characteristic equations is given in Remark 4.2.

[6]The characteristic equations may be formulated so that the independent variable does not involve either the stress or strain rate, but since we seek stress as a function of strain rate, it simplifies the exposition to

reformulate them so that one component of the strain rate, the magnitude of the deviatoric strain rate s, is the independent variable.

[7]We use the same letters to denote real variables, as in equation (4.5), and to denote functions of s, as in equations (4.6). In the hope of warding off confusion, from here on we underline a letter when it denotes a *function*. Even though the p-equation in equations (4.6) is trivial, we still underline p when it is part of a solution of equations (4.6). Although equations (4.6) depend on ϕ, here and below our notation for solutions of the equations does not indicate this dependence.

[8]Note that the right-hand side of equation (4.23) is singular at the initial point since both numerator and denominator vanish there, hence, despite equation (4.23) being a first-order ODE, both the initial point and initial derivative must be specified. The condition on the derivative uses the eigenvector (4.17) to pick out an initial direction for which a differentiable solution of the IVP exists i.e. the unstable manifold of equations (4.13) originating at E_-.

[9]We do not specify φ in equation (4.32) because it is undefined along this axis.

[10]Given a symplectic manifold (M, ω) of dimension $2m$, let $N \subset M$ be a submanifold satisfying $\omega|_N = 0$. It is a well-known fact in symplectic geometry that $\dim(N) \leq m$. When $\dim(N)$ is exactly m, N is called a Lagrangian submanifold of (M, ω). See [38, pp. 566 and 568] for more detail.

References

1. Onsager L. 1931 Reciprocal relations in irreversible processes. I. *Phys. Rev.* **37**, 405–426. (doi:10.1103/PhysRev.37.405)
2. Doi M. 2011 Onsager's variational principle in soft matter. *J. Phys. Condens. Matter* **23**, 284118. (doi:10.1088/0953-8984/23/28/284118)
3. Goddard JD. 2014 Edelen's dissipation potentials and the visco-plasticity of particulate media. *Acta Mech.* **225**, 2239–2259. (doi:10.1007/s00707-014-1123-3)
4. Jiang Y, Liu M. 2009 Granular solid hydrodynamics. *Granul. Matter* **11**, 139–156. (doi:10.1007/s10035-009-0137-3)
5. Edelen DGB. 1972 A nonlinear onsager theory of irreversibility. *Int. J. Eng. Sci.* **10**, 481–490. (doi:10.1016/0020-7225(72)90091-2)
6. Goddard J, Lee J. 2018 Regularization by compressibility of the μ(I) model of dense granular flow. *Phys. Fluids* **30**, 073302. (doi:10.1063/1.5040776)
7. Chialvo S, Sun J, Sundaresan S. 2012 Bridging the rheology of granular flows in three regimes. *Phys. Rev. E* **85**, 021305. (doi:10.1103/PhysRevE.85.021305)
8. BagnoldRA. 1954 Experiments on a gravity-free dispersion of large solid spheres in a newtonian fluid under shear. *Proc. R. Soc. Lond. A. Math. Phys. Sci.* **225**, 49–63. (doi:10.1098/rspa.1954.0186)
9. MiDi GDR. 2004 On dense granular flows. *Eur. Phys. J. E.* **14**, 341–365. (doi:10.1140/epje/i2003-10153-0)
10. da Cruz F, Emam S, Prochnow M, Roux JN, Chevoir F. 2005 Rheophysics of dense granular materials: discrete simulation of plane shear flows. *Phys. Rev. E* **72**, 021309. (doi:10.1103/PhysRevE.72.021309)
11. Pouliquen O, Cassar C, Jop P, Forterre Y, Nicolas M. 2006 Flow of dense granular material: towards simple constitutive laws. *J. Stat. Mech.* **2006**, P07020–P07020. (doi:10.1088/1742-5468/2006/07/P07020)
12. Barker T, Schaeffer D, Shearer M, Gray J. 2017 Well-posed continuum equations for granular flow with compressibility and μ(I)-rheology. *Proc. R. Soc. A* **473**, 20160846. (doi:10.1098/rspa.2016.0846)
13. Lagioia R, Panteghini A. 2016 On the existence of a unique class of yield and failure criteria comprising Tresca, von Mises, Drucker–Prager, Mohr–Coulomb, Galileo–Rankine, Matsuoka–Nakai and Lade–Duncan. *Proc. R. Soc. A* **472**, 20150713. (doi:10.1098/rspa.2015.0713)
14. Lode W. 1926 Experiments on the Influence of the mean principal stress on the flow of the Metals Iron, Copper and Nickel. *J. Phys.* **36**, 913–939. (doi:10.1007/BF01400222)
15. Rauter M, Barker T, Fellin W. 2020 Granular viscosity from plastic yield surfaces: the role of the deformation type in granular flows. *Comput. Geotech.* **122**, 103492. (doi:10.1016/j.compgeo.2020.103492)

16. Schaeffer DG, Barker T, Tsuji D, Gremaud P, Shearer M, Gray JMNT. 2019 Constitutive relations for compressible granular flow in the inertial regime. *J. Fluid Mech.* **874**, 926–951. (doi:10.1017/jfm.2019.476)
17. Clemmer JT, Srivastava I, Grest GS, Lechman JB. 2021 Shear is not always simple: rate-dependent effects of flow type on granular rheology. *Phys. Rev. Lett.* **127**, 268003. (doi:10.1103/PhysRevLett.127.268003)
18. Kim S, Kamrin K. 2023 A second-order non-local model for granular flows. *Front. Phys.* **11**, 1092233. (doi:10.3389/fphy.2023.1092233)
19. Radjai F, Delenne JY, Azéma E, Roux S. 2012 Fabric evolution and accessible geometrical states in granular materials. *Granul. Matter* **14**, 259–264. (doi:10.1007/s10035-012-0321-8)
20. Pouliquen O, Forterre Y. 2009 A non-local rheology for dense granular flows. *Phil. Trans. R. Soc. A* **367**, 5091–5107. (doi:10.1098/rsta.2009.0171)
21. Kamrin K, Koval G. 2012 Nonlocal constitutive relation for steady granular flow. *Phys. Rev. Lett.* **108**, 178301. (doi:10.1103/PhysRevLett.108.178301)
22. Berzi D. 2024 On granular flows: from kinetic theory to inertial rheology and nonlocal constitutive models. *Phys. Rev. Fluids* **9**, 034304. (doi:10.1103/PhysRevFluids.9.034304)
23. Sun J, Sundaresan S. 2011 A constitutive model with microstructure evolution for flow of rate-independent granular materials. *J. Fluid Mech.* **682**, 590–616. (doi:10.1017/jfm.2011.251)
24. Truesdell C, Noll W. 1965 *The non-linear field theories of mechanics*. Springer, New York, USA. (doi:10.1007/978-3-642-46015-9_1)
25. Lubliner J. 1990 *Plasticity theory*. Harlow, UK: Pearson Education.
26. Spencer AJM. 1980 *Continuum mechanics*. Harlow, UK: Longman.
27. Heyman J, Delannay R, Tabuteau H, Valance A. 2017 Compressibility regularizes the μ(I)-rheology for dense granular flows. *J. Fluid Mech.* **830**, 553–568. (doi:10.1017/jfm.2017.612)
28. Jop P, Forterre Y, Pouliquen O. 2006 A constitutive law for dense granular flows. *Nature* **441**, 727–730. (doi:10.1038/nature04801)
29. Srivastava I, Silbert LE, Grest GS, Lechman JB. 2021 Viscometric flow of dense granular materials under controlled pressure and shear stress. *J. Fluid Mech.* **907**, A18. (doi:10.1017/jfm.2020.811)
30. Hinch EJ, Leal LG. 1975 Constitutive equations in suspension mechanics. Part 1. General formulation. *J. Fluid Mech.* **71**, 481–495. (doi:10.1017/S0022112075002698)
31. Walton OR, Braun RL. 1986 Stress calculations for assemblies of inelastic speres in uniform shear. *Acta Mech.* **63**, 73–86. (doi:10.1007/BF01182541)
32. Alam M, Luding S, Garcia-Rojo R, Herrmann H, McNamara S. 2005 Non-newtonian granular fluid: simulation and theory. In *Powders and grains* (ed. S McNamara), pp. 1141–1144.
33. Saha S, Alam M. 2016 Normal stress differences, their origin and constitutive relations for a sheared granular fluid. *J. Fluid Mech.* **795**, 549–580. (doi:10.1017/jfm.2016.237)
34. Maklad O, Poole RJ. 2021 A review of the second normal-stress difference; its importance in various flows, measurement techniques, results for various complex fluids and theoretical predictions. *J. Nonnewton. Fluid Mech.* **292**, 104522. (doi:10.1016/j.jnnfm.2021.104522)
35. Bryant RL, Chern SS, Gardner RB, Goldschmidt HL, Griffiths PA. 1991 *Exterior differential systems*. vol. **18**. New York: Mathematical Sciences Research Institute Publications. Springer-Verlag.
36. Barker T, Gray JMNT, Schaeffer DG, Shearer M. 2023 Well-posedness and ill-posedness of single-phase models for suspensions. *J. Fluid Mech.* **954**, A17. 10.1017/jfm.2022.1004. (doi:10.1017/jfm.2022.1004)
37. Hu Y, Schaeffer D, Barker T. 2024 Supplementary material from: Onsager-symmetric constitutive laws for 3D granular flow in the inertial regime. Figshare. (doi:10.6084/m9.figshare.c.7577968)
38. Lee JM. 2013 *Introduction to smooth manifolds*, 2nd ed. New York, USA: Springer. (doi:10.1007/978-1-4419-9982-5_1)